Received: 12 November 2023 | Revised: 8 June 2024 | Accepted: 3 August 2024

DOI: 10.1002/gj.5046

WILEY

RESEARCH ARTICLE

Magnetostratigraphy and rock magnetic studies on the Cretaceous-Paleogene transition strata along the Um Sohryngkew River, Therriaghat, Meghalaya, India

Debarati Nag[1] | Satish J. Sangode[1] | Sarvendra P. Singh[2] | Prem R. Uddandam[2] | Adrita Choudhuri[2] | Binita Phartiyal[2] | Vandana Prasad[2]

[1]Department of Geology, Savitribai Phule Pune University, Pune, India

[2]Birbal Sahni Institute of Palaeosciences, Lucknow, India

Correspondence
Debarati Nag, Department of Geology, Savitribai Phule Pune University, Ganeshkhind Rd, Pune 411007, India.
Email: debarati_nag@yahoo.co.in

Vandana Prasad, Birbal Sahni Institute of Palaeosciences, 53-University Road, Lucknow 226007, India.
Email: prasad.van@gmail.com

Handling Editor: M. Ramkumar

A combination of magnetic polarity and rock magnetic analysis on the well-documented section of the Um Sohryngkew River (USR) in the south Shillong Plateau, NE India, produced a sharp reversal marking the C29r-C29n geomagnetic polarity transition at approximately 65.688 Ma. The rock magnetic studies indicate ferrimagnetic dominant mineralogy with abundance of SSD grains, with an anomalous peak in susceptibility coinciding with Ir-rich limonitic layer. The magnetic reversal occurs precisely 61 m above the Ir-rich distinct in situ limonitic layer, indicating that the C29r-C29n geomagnetic reversal post-dates the widely accepted Ir-anomaly based K-Pg boundary by approximately 355 Ka. Furthermore, the rock magnetic studies indicate its frequency dependence coinciding with the Ir-rich limonitic layer suggesting a possible dust/aerosol source, while akaganéite is reported from the interval approximately 1 m below peak susceptibility, indicating signature of Deccan volcanism. This study infers the completeness of the USR section with a high rate of sedimentation of approximately 17 cm/ka among the marine K-Pg boundary sections in the world.

KEYWORDS
aerosol, akaganéite, bollide impact, Deccan volcanism, K-Pg boundary, magnetic susceptibility, Meghalaya

1 | INTRODUCTION

The Cretaceous-Paleogene (K-Pg) transition represents a significant period in Earth's geologic history being associated with one of the most important mass extinctions that laid foundations for the Cenozoic and modern life forms. Although the K-Pg mass extinction has been subjected to extensive research, there remains many unresolved aspects pertaining to the type (gradual or abrupt) and causes of the extinction (Bernaola et al., 2006). A series of events such as the Chixulub impact and Deccan Trap volcanism occurring during the short interval of the K-Pg transition renders it difficult to isolate the exact cause of the extinction event and climatic variations (L. W. Alvarez, 1980; W. Alvarez et al., 1984; Chenet et al., 2009; Courtillot et al., 1988; Keller et al., 2003, 2004; Renne et al., 2013, 2015; Schoene et al., 2015). A more comprehensive study of the biological, sedimentological and climatic changes recorded within a sedimentary sequence during the boundary interval is still needed to better understand the causes of extinction and the subsequent recovery dynamics.

In India, some marine Cretaceous-Paleogene sections have been identified, although most of these sections do not demonstrate continuity of the Maastrichtian-Danian sequence (N. Bhandari et al., 1993). The Um Sohryngkew River (USR) section in the south Shillong Plateau, NE India, represents a well-established complete marine K-Pg sedimentary sequence (M. Bhandari et al., 1994; Garg & Jain, 1995; Gertsch et al., 2011; Lahiri et al., 1988; Mukhopadhyay, 2008; Pandey, 1990), for which precise chronostratigraphy is awaited. Being proximal to the Deccan Volcanic Province (DVP), the study site can address the ongoing debate on volcanism versus asteroidal impact of

the K-Pg extinction, in addition to its application for regional and global correlations. To decipher the environmental and climatic changes linked to the K-Pg transition period, it is thus necessary to recognize the imprints of bolide impact and volcanic markers in sedimentary rock records and correlate their stratigraphic position relative to the K-Pg boundary (Font & Bond, 2021). Apart from several other approaches, magnetostratigraphy is one of the most suited methods to document the K-Pg over the exposed lithounits spanning within the C29r magnetozone (Cande & Kent, 1995). Despite being such a geologically critical and significant exposure, magnetic polarity data for the USR section are not available. This work presents the first magnetostratographic attempt on the USR section producing the palaeomagnetic data of the K-Pg section in Meghalaya. Here, we present the detailed demagnetization data with discussions on the palaeomagnetic directions revealed based on 57 oriented block samples collected from the 105 m-long USR section.

In the USR section, the K-Pg boundary is considered to be synchronous with a 1.5 cm thick limonitic layer enriched with iridium (Ir) and platinum group of elements (PGEs) within the Mahadek Formation (N. Bhandari et al., 1987). Pandey (1990), however, suggested that the K-Pg boundary interval ranges from 1.5 m below to 0.5 m above the Ir-rich layer based on gradual biostratigraphic changes and the presence of Cretaceous planktonic foraminifera *Geumbelitria cretacea* above the Ir layer. While Garg and Jain (1995) based on the Maastrichtian nanofossil marker, *Micula prinsii*, stated that the K-Pg boundary occurs just below the Ir-rich layer near the Mahadek-Langpar contact. In contrast, from the same section, Mukhopadhyay (2008) reported that the K-Pg boundary occurs approximately 6.6 m above the Ir-rich layer, while Lahiri et al. (1988) placed the boundary 30 m above the Ir layer. The controversies regarding the age demarcation within the same sedimentary sequences from the Shillong Plateau further necessitate the use of chronostratigraphic methods that are independent of lithostratigraphy and biostratigraphy, such as magnetostratigraphy. The above information, however, hints towards continuity of the section to precisely record the K-Pg boundary without any traceable gap in sedimentation, which is better suited for recording of the magnetic polarity. This study thus develops the magnetostratigraphy of the sedimentary sequence and attempts to decipher the signature of volcanism and bollide impact through the integration of rock magnetic signals and previously developed litho- and geochemical records. Dinoflagellate cysts have also been studied on selective samples; however, detailed high-resolution data are awaited.

2 | GEOLOGICAL SETTING AND LITHOLOGY

The Shillong Plateau in northeastern India is a fault-bounded 'pop-up' structure and signifies a cut-off patch of the Indian Peninsular Shield (Desikachar, 1974; England & Bilham, 2015; Govin et al., 2018). It is bordered by the Dauki Fault in the south, the Brahmaputra lineament towards the north, the Naga-Disang Schuppen Belt to the east and the Dhubri lineament towards the west (Desikachar, 1974; Evans, 1964). The plateau covers an area of approximately 47,614 km^2 within 25°12′ N–26°45′ N latitude and 91°30′ E–92°20′ E longitude (Devi & Sarma, 2010). The region comprises the Precambrian crystalline basement rocks, the Proterozoic Shillong Group of metasedimentary rocks and metavolcanic rocks intruded by the Neoproterozoic granite plutons (S. K. Ghosh et al., 1994; GSI, 2009; Mitra, 1998). The plateau has also recorded Permo-Carboniferous Gondwana sedimentation towards the west, the Early Cretaceous basaltic traps (Sylhet Traps) and the continuous sedimentation since the Late Cretaceous to Paleogene along the southern margin of the plateau (Ali & Duarah, 2022) (Figure 1). The present study focuses on the Late Cretaceous–Paleogene sediment sequence exposed along the Um Sohrynkew River near Therria village, South Shillong Plateau in the East Khasi Hills district.

The Cretaceous–Paleogene sediment sequence, which is exposed on the western and southern fringe of the plateau, has been studied in detail for the development of stratigraphic frameworks by previous workers (Bhattacharyya & Bhattacharya, 1981; Biswas, 1962; Chakraborty & Bakshi, 1972; A. M. N. Ghosh, 1940; Lahiri et al., 1988; Medlicott, 1869; Murthy et al., 1976; Nagappa, 1959; Pandey, 1981). The studied sedimentary sequence comprises the topmost Mahadek Formation of the Khasi Group and the Langpar Formation of the Jaintia Group. The upper part of the Mahadek Formation represents an upper shelf environment characterized by coarse- to medium-grained calcareous arenaceous facies and glauconitic sandstone, indicating marine transgression, while the Langpar Formation is dominated by calcareous shale, carbonaceous shale and argillegeous limestone from a deeper shelf environment (Dalabehera et al., 2021; Mishra & Sen, 2001).

The investigated section comprising the upper Mahadek and Langpar formations is exposed along both the banks of the Um Sohryngkew River (Figure 1b). The section consists of tilted strata with a 25–35° southeastward dip. The lithology of the studied section is divided into five units (Figure 2) and exposed along both the banks of the river (Figure 2b,c). Based on the lithological characteristics, the lower 20 m of the sequence is referred to as Unit 1 and consists of dominantly sandstone beds with fossiliferous horizons (ammonites, gastropods, bivalves) (Figure 2d) and at some places alternated with argilleceous beds. Unit 1 is identified as the Upper Mahadek Formation and is exposed along the east bank of the Um Sohryngkew River. This is followed by approximately 15 m of the sequence eroded from the east bank; however, a portion of this 15 m eroded part (~3 m) is recorded from the western bank referred to as Unit 2. The basal part of Unit 2 consists of approximately 1 m thick mudstone bed that contains two limonitic clay beds of approximately 2 cm and approximately 20 cm thickness. The lower limonitic clay bed hosts a reddish layer that corresponds to the iridium layer of N. Bhandari et al. (1987) and M. Bhandari et al. (1994) (Figure 2e). The lower part is overlain by approximately 2 m thick alternating calcareous shale beds and limestone bands. Unit 2 is included in the Mahadek Formation according to some authors (Pandey, 1990), while others conclude this to be part of the Langpar Formation (Garg & Jain, 1995). Thereafter, the sediment sequence above Unit 2 in the west bank is either eroded or is

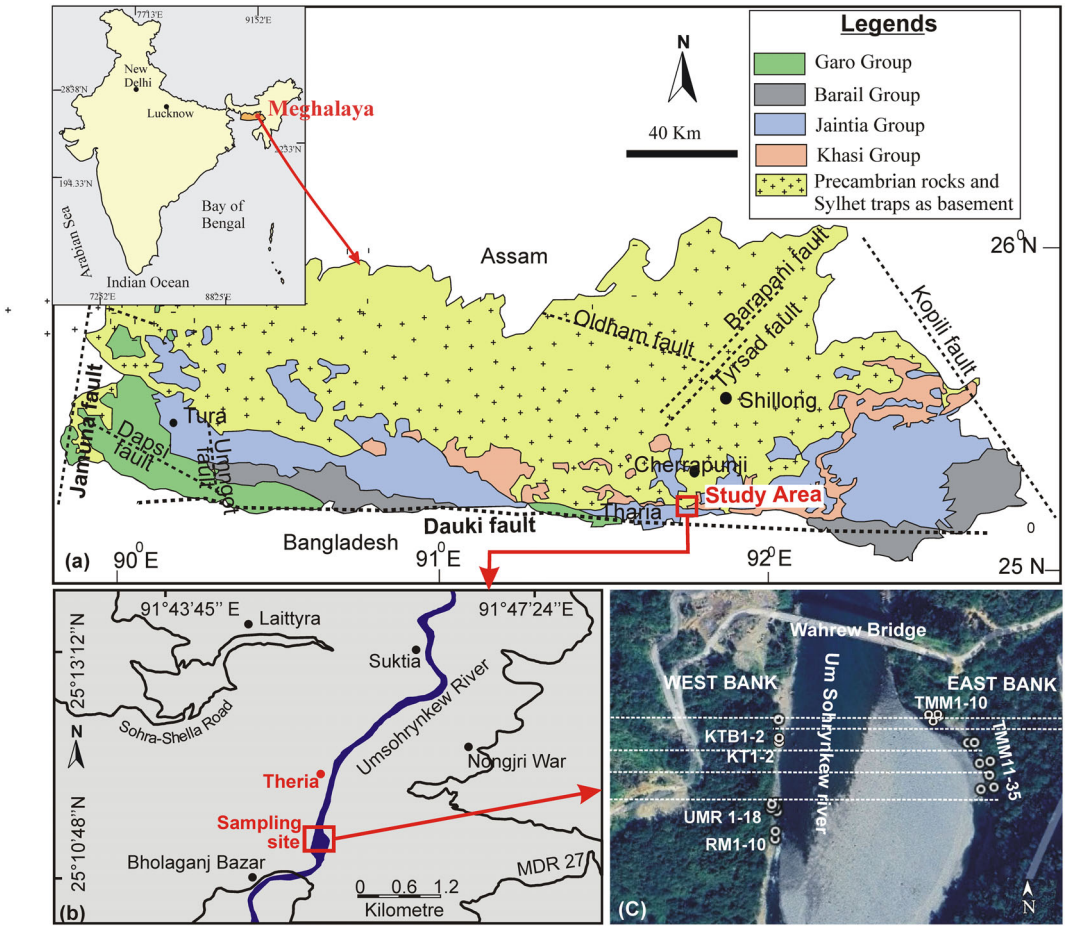

FIGURE 1 (a) Geological map of Shillong Plateau of Meghalaya state of India (modified after GSI, 2009) showing the exposed Cretaceous-Tertiary sediments and the study location. (b) Location of the sampling site near the Therria village in Shillong along the Um Sohrynkew River. (c) Google Earth image of the Um Sohrynkew River section with the global positioning system locations of the magnetostratigraphic sampling sites exposed on both banks of the river.

unexposed under dense vegetation. Stratigraphically equivalent and younger sediments are therefore sampled from the east bank by precise tape and compass surveys and bed matching. This unit is represented as Unit 3, which is an approximately 47 m thick argillaceous shale bed with intercalating limestone bands. This is followed by younger Units 4 and 5, approximately 20 m thick, consisting of alternating shale and limestone beds of variable thickness that are again documented from the West Bank. Unit 4 is more argillaceous, while Unit 5 is dominated by limestone beds. In the present study, Unit 1 is the topmost Mahadek Formation, while Units 2 to 5 are considered as the Langpar Formation based on the lithological composition consisting of dominantly argillaceous and limestone beds.

3 | MATERIALS AND METHODS

The exposed outcrops are mapped by traversing along the Um Sohryngkew River, where the Cretaceous–Paleogene sediment sequence is exposed along both banks. A detailed litholog is prepared to understand the changes in lithology and plan the magnetostratigraphic sampling. The positions of the sedimentary beds on both banks are traced with the help of bed tracing, tape and compass survey and global positioning system (GPS) measurements and plotting them on Google Earth. Magnetostratigraphic sampling is performed from relatively undisturbed, less weathered, well-exposed sediment beds. A total of 57 oriented block samples are collected from the approximately 105 m thick sequence following standard palaeomagnetic procedures. For each block sample, a flat surface is created for marking north on the top surface and spirit level horizontal marks on the adjacent vertical sides for reference during laboratory reorientation. The spacing between the sampling levels varied from approximately 1 to approximately 7 m depending on the availability of suitable sediment beds.

The block samples are reoriented in the laboratory, and cores are drilled by a Lapidary rock drill to obtain cylindrical cores 6–8 cm in length. Three to four cylindrical cores are extracted from each block, which is then further subsampled into 331 standard palaeomagnetic specimens of approximately 2.2 cm length and 2.54 cm diameter using an ASC Scientific dual blade rock saw. All the specimens are measured for bulk magnetic susceptibility (χ) and natural remanent

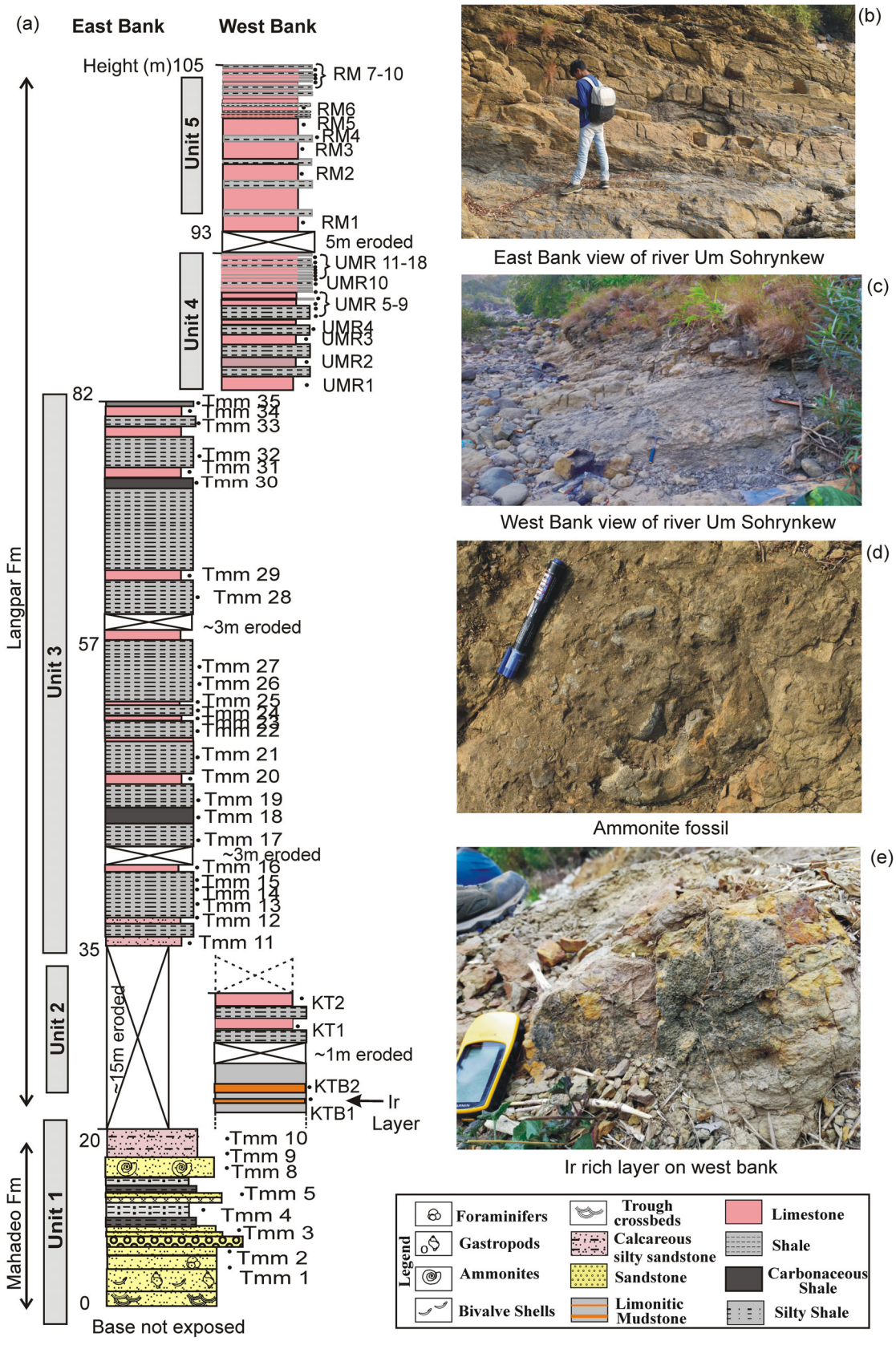

FIGURE 2 (a). Litholog of the studied sedimentary sequence divided into five units. (b) Overview of the Langpar Formation showing alternation between shale and calcarenite beds from the east (right) bank of the Um Sohryngkew River. (c) The exposed beds from the west (left) bank of the river. (d) Ammonite fossil from the sandstone bed of Upper Mahadek Formation. (e) Close-up view of the Ir-rich limonitic bed from the west (left) bank of the river.

magnetization (NRM); thereafter, the Königsberger ratio 'Q' (Königsberger, 1938) is calculated to test the stability of specimens for palaeomagnetic analysis. For magnetic cleaning, the specimens are subjected to alternating field demagnetization (AFD) using a D2000 alternating field demagnetizer and thermal demagnetization (TD) of an ASC Scientific TD-48 thermal demagnetizer to isolate the characteristic remanent magnetization (ChRM) components. The AFD is carried out in 19 progressive steps up to 160 mT, and the TD is given 17 progressive steps from 80° to 700°C with continuous monitoring of magnetic susceptibility. After demagnetizing at any particular temperature, the samples are cooled to room temperature in a near zero magnetic field before measuring the remanent magnetizations. The remanence is measured in a JR-6 spinner magnetometer with a sensitivity of 2×10^{-6} A/m (AGICO, Czech Republic) to obtain the remanent vectors, moment and directions (*D*, *I* and intensity). The demagnetization behaviour of the specimens is presented in the form of vector end-point diagrams (Zijderveld plots) (Zijderveld, 1967) and decay of intensity in the course of demagnetization steps. The demagnetization data are processed with the AGICO Remasoft 3.0 program (Chadima & Hrouda, 2006) by applying principal component analysis (Kirschvink, 1980) to obtain the ChRM directions. Mean directions and their α_{95} (95% confidence angle) are obtained by Fisher statistics (Fisher, 1953), and virtual geomagnetic poles (VGP) for each sample are calculated by using tilt corrected mean declination and inclinations on successfully demagnetized specimens by using PMGSC software (Enkin et al., 2003).

Rock magnetic measurements are performed to assess the characteristics of the magnetic minerals essential for recording primary remanence magnetization. For rock magnetic analysis, the samples are packed into standard non-magnetic plastic bottles of 10 cm^3. Low-frequency (0.47 kHz) and high-frequency (47 kHz) magnetic susceptibility (χ_{lf}) are measured using a Bartington magnetic susceptibility meter and MS2B dual-frequency sensor. Anhysteretic remanent magnetization (ARM) is imparted using a peak AF demagnetization field of 100 mT with a superimposed DC bias field of 0.05 mT using a D2000T AF demagnetizer and expressed as susceptibility of ARM (χ_{ARM}), which is sensitive to the concentration of single domain (SD) ferrimagnetic grains in the 0.02–0.4 μm range (Maher, 1988). Isothermal remanent magnetization (IRM) is induced in the samples at different field strengths of 20, 50, 70, 100, 200, 300, 500, 800 up to 1000 mT and back fields up to −300 mT using an ASC Scientific IM 10–30 Impulse Magnetizer. Additionally, different interparametric ratios χ_{fd}%, SIRM/χ_{lf}, χARM/SIRM, S-ratio and HIRM are calculated. The S-ratio is calculated by the expressions ($-IRM_{-300mT}$/$SIRM_{1000mT}$) and the HIRM as ($IRM_{-300} + SIRM$)/2 (Q. S. Liu et al., 2007). The measurement of the temperature dependence of magnetic susceptibility ($\chi - T$) is carried out in a temperature range of 40 to 700°C using a Bartington MS2W sensor. The samples are heated in MS2WF furnace system, and the Geolabsoft software package is used to collect data and display the results during the measurement. Small sediment chunks are used for this analysis.

Fresh selected rock fragments are observed under a JSM 1076F SEM microscope coupled to an energy dispersive spectra (EDS) detector. The electron source for the SEM is a tungsten wire. JSM 1076F utilizes SEM mode for high-resolution images at accelerating voltages of 0.5 to 30 kV. Compositional analysis is provided by EDS by using EDAX make LN2 free, Peltier cooled, Octane plus model (30 mm^2 and 127 eV resolution) with TEAM software. Representative samples are also studied for dinoflagellate cysts and other organic matter remains from each unit. Samples are prepared following standard palynological techniques, including treatment with HCl, HF and KOH, washing and sieving. The palynological content is examined using a DM 2500 Leica Microscope.

4 | RESULTS

4.1 | Rock magnetic analysis

The χ_{lf}, χ_{ARM}, χ_{ARM}/χ_{lf}, IRM, S-ratio, Soft-IRM and Hard-IRM along with the temperature-dependent ($\chi - T$) susceptibility are inferred to identify the magnetic mineralogy and grain size for the sediment samples.

The bulk low-frequency magnetic susceptibility (χlf) for 331 specimens varies from 3.6 to 17.94 $\times 10^{-8}$ m^3 kg^{-1}, indicating a moderate to weak ferrimagnetic nature of the specimens. The carbonate-dominant mineralogy producing the diamagnetic effect also appears to be responsible for the low magnetic susceptibility. However, within this background, the magnetic susceptibility has shown two anomalous peaks. The first peak (peak-1) occurs at sample numbers 7 (KTB1) and 8 (KTB2) in Unit 2, coinciding with the Ir-rich layer, and the second peak (peak-2) occurs for samples 33–36 (UMR1 to UMR4) within Unit 4 (Figure 3). The bell-shaped peak-1 does not match any of the other parameters, such as SIRM, HIRM, Soft-IRM and χ_{ARM}. However, this peak is marked by a major change in the mineral composition by a change from dominant antiferromagnetic (Unit 1) to ferrimagnetic minerals (Unit 2). Lithologically, there is a major change in the facies from sandstone dominant to mudstone-silt dominating sequence above. The samples showing peak 1 (KTB1 and KTB) encased within the bell-shaped peak are distinctly limonitic. Limonite, having compositions similar to ferrihydrites, should reflect weak antiferromagnetic characters to impart low susceptibility signatures (Schwertmann & Taylor, 1989). The high magnetic susceptibility along with low SIRM and coercivity clearly depict the presence of the SP fraction. Furthermore, there is an anomalous peak in χfd%, confirming the SP ferrimagnetic enrichment, which can be of aerosol origin, as anticipated in the K-Pg event. For Peak-2 high susceptibility correspond to increased χ_{ARM} at this interval. Furthermore, there is no peak in χfd%, thus indicating the effect of the depositional environment on enriching the SD ferrimagnets (Figure 3). The base of the sequence shows high χ_{ARM} due to the high concentration of stable single domain (SSD) grains. Thereafter, the χ_{ARM} drops for the entire sequence from samples 4 to 28 (TMM8 to TMM31, Units 2 and 3), within a range from 2.56 to 6.34 $\times 10^{-8}$ A m^2 kg^{-1}. The χ_{ARM} and χ_{ARM}/χ_{lf} values for these samples indicate magnetic grain sizes ranging from SSD to pseudo single domain (PSD). χ_{ARM} values fluctuate but greatly increased from

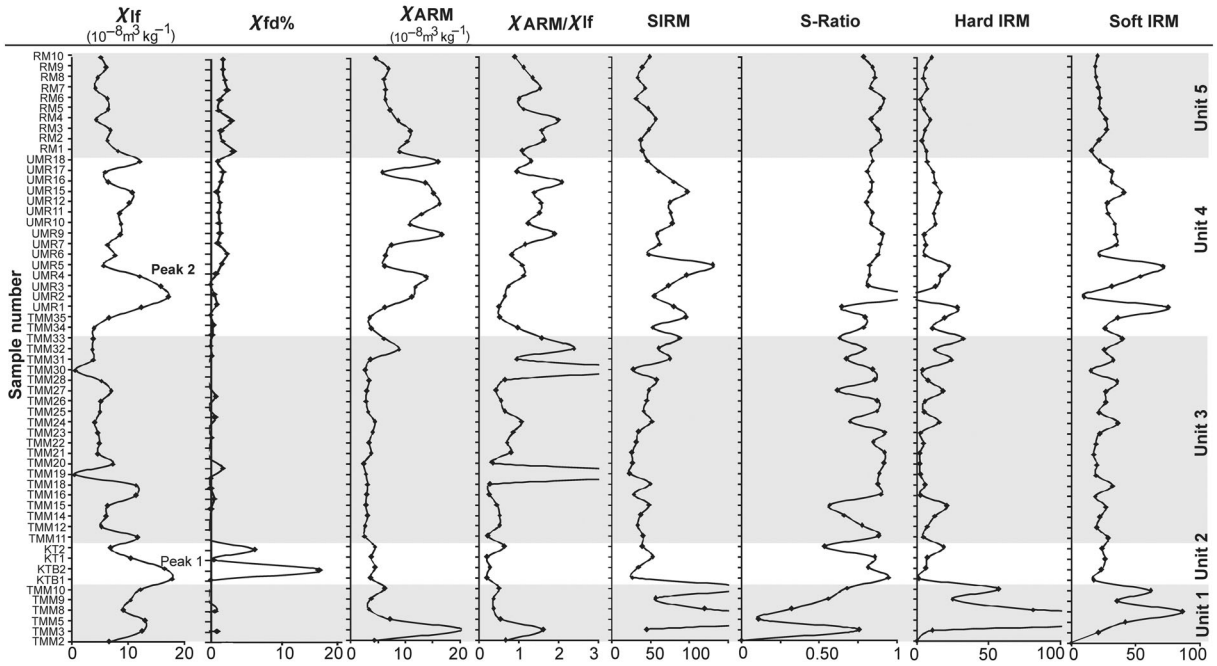

FIGURE 3 Rock magnetic parameters depicting magnetic concentration, mineralogy and grain size for sediment samples from the five lithological units.

sample 29 (TMM32; Unit 4), with a slight decrease in topmost 10 samples (Unit 5). This is also corroborated by χ_{ARM}/χ_{lf}, whereby except for a few peaks in the lower part, higher values are present from sample 29 and thereafter indicating presence of SSD to PSD magnetic grain size. SIRM shows the concentration of ferrimagnetic content and does not follow the trend of magnetic susceptibility. The SIRM plot shows a fairly good contribution from ferrimagnetic mineralogy. The S ratio of near 1 and both soft and hard IRM components also shows the presence of ferrimagnetic minerals for Units 2, 4 and 5 (Figure 3). For Unit 1, the S-ratio, HIRM and Soft-IRM indicate a mixed magnetic mineralogy with a high contribution from antiferromagnetic minerals, while for Unit 3, the mixed magnetic mineralogy is seen with dominance of ferrimagnetic minerals.

The $\chi - T$ curves are helpful in the identification of the magnetic mineral phases present in the samples (C. L. Deng et al., 2001; Q. Liu et al., 2005). Representative $\chi - T$ curves of the selected samples from the studied section are shown in Figure 4a–g. Sample TMM2 from Unit 1 shows an increase in χ with temperature, forming a peak at approximately 150°C; thereafter, it decreases with two drops at 300 and 475°C and becomes zero at 680°C, indicating the presence of both ferri (maghemite/Ti-magnetite/magnetite-like phases) and the antiferromagnetic (goethite, haematite) phase, while the low susceptibility for the cooling curve may indicate maghemite to haematite conversion. For Unit 2 (KTB1), the broad susceptibility peak at 300°C (T_{c1}) in the heating curve with a final drop at 680°C indicates the presence of maghemite and haematite with an inversion effect. The increase in susceptibility during heating can be attributed to the neoformation of the ferrimagnetic phase from Fe-containing silicates and clays (C. Deng et al., 2004). Lower susceptibility for the cooling curve and absence of (T_{c1}) shows thermal alteration from the soft magnetic phase to the hard magnetic phase. For samples from Unit 3 (TMM 11 and TMM 14), a drop in Curie temperatures was observed at 450–500°C, suggesting that titanium-poor Ti-magnetite and residual magnetic susceptibility becomes effectively zero at 680°C, indicating a minor haematite content (Dannemann et al., 2022). For TMM 25 (Unit 3), the heating curve with a Curie temperature between 300 and 400°C indicates titanium-rich Ti-magnetite, and the drop at 680°C again suggests the presence of haematite. Two humps can be seen for TMM25, indicating transformation to a higher susceptibility phase because of the heating process. Unit 4 (UMR4) shows almost reversible heating and cooling curves and indicates no significant alteration due to heating. A drop in Curie temperature is seen between 375 and 500°C, while a small drop is seen at 680°C, showing the dominance of ferrimagnetic minerals (maghemite/Ti-magnetite/magnetite) and a minor contribution from haematite. The heating curve for Unit 5 (RM7) shows drops at 450 and 500°C, indicating Ti-magnetite/magnetite and minor haematite with a drop at 680°C, while the higher susceptibility for the cooling curve indicates the transformation of Ti-magnetite to magnetite.

IRM acquisition has been carried out for selected samples from each unit (Figure 4h). Unit 1 (TMM 5 and TMM 9) shows IRM acquisition to remain unsaturated at 1000 mT, depicting the dominance of hard magnetic (antiferromagnetic) minerals, which is also supported by the S ratio and HIRM. Samples TMM5 and TMM9 from Unit 1 with a $B_{(o)CR}$ value of 119 mT indicate the dominance of a high coercive component as well. The samples from Unit 3 (TMM 15, TMM 25, KTB1, KT2) show mixed magnetic mineralogy achieving saturation at approximately 700 mT. Progressive removal of SIRM by applying

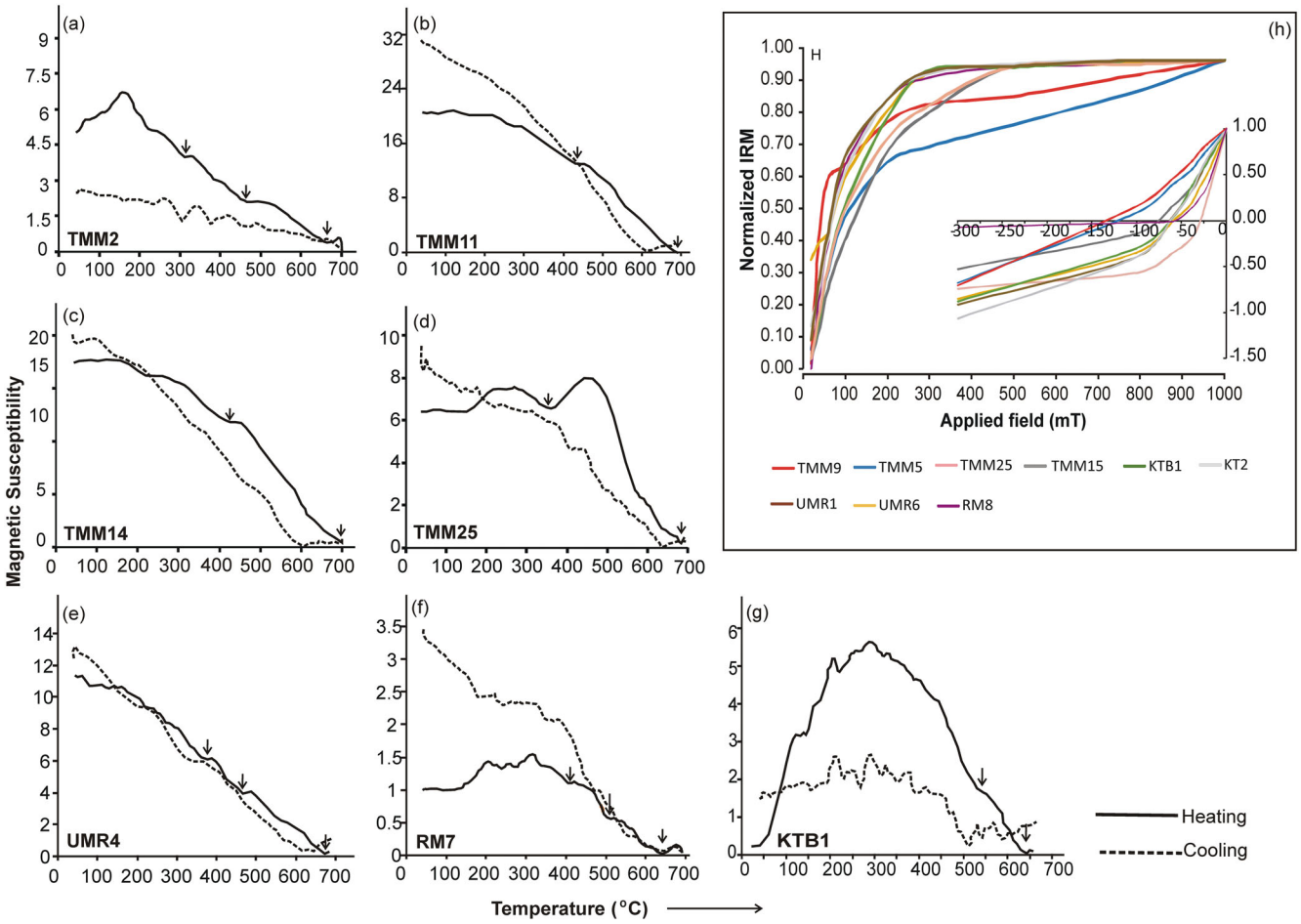

FIGURE 4 (a–g) Thermomagnetic curves indicating plot of temperature and magnetic susceptibility ($\chi - T$) for the selected samples from the Um Sohrynkew sediment sequence. (h) Isothermal remanent magnetization curves for the representative samples for both forward (till 1000 mT) and backward fields (till −300 mT).

reverse fields yielding coercivity of remanence ($B_{(0)CR}$) ranging between 26 and 75 mT for most of the samples suggests dominance of SSD to PSD Ti-magnetite and magnetite and minor contributions of haematite. The IRM acquisition curves for the samples from Units 3, 4 and 5 (KTB1, KT2, UMR1, UMR6, RM8) show saturation near 300 mT, indicating the presence of soft ferrimagnetic minerals, and $B_{(0)CR}$ values range from 62 and 65 mT, indicating SSD to PSD grain size.

4.2 | SEM–EDS

Scanning electron microscopy (SEM) observations coupled to energy dispersive spectroscopy (EDS) analyses are conducted particularly to verify the presence of the mineral akaganéite in the USR sedimentary sequence. This mineral is targeted since akaganéite, which is a Cl-bearing iron (hydro) oxide is considered a volcanic marker for the K-Pg boundary. SEM–EDS analysis is focused for samples in the USR sedimentary sequence from units 1, 2 and lower part of Unit 3 and around the portion that includes Peak-2 of Unit 4. SEM–EDS analysis reveals the presence of a mineral containing Cl in association with Fe oxide. This mineral occurred as very small discrete crystals with sub-hedral flat shapes from samples TMM9 and TMM10 (Unit 1) below the peak magnetic susceptibility interval (Peak-1) of around 1–4 wt% and <200 μm size. The samples from near Peak-2 (Unit 4) do not show any record of this mineral and thus are excluded from further discussion. Framboidal pyrite of less than 10 μm and some trace elements, such as V, Cr and P, are also observed in SEM–EDS from Peak-1. Representative images and data are presented in Figures 5 and 6.

4.3 | Dinoflagellate cysts

The preservation of dinoflagellate cysts varies between poor and moderate (Figure 7). Unit-1 consists of a negligible amount of organic matter or no organic matter, revealing low productivity and unsuitable facies, that is, sandstone with well-ventilated conditions resulting in rapid degradation of organic matter. Unit 2 consists of high abundances of dinoflagellate cysts representative of late Maastrichtian

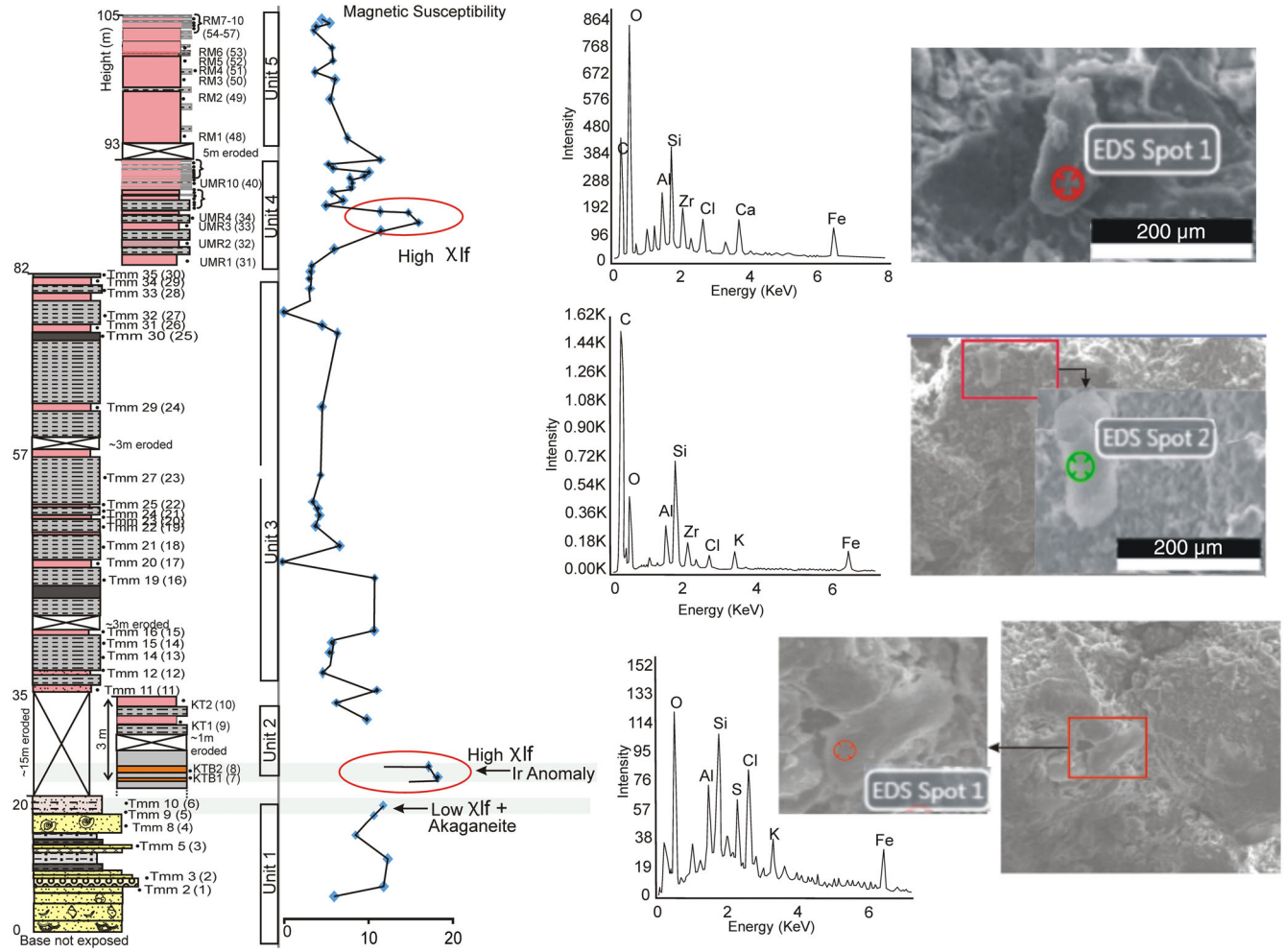

FIGURE 5 Scanning electron microscopy images of the akaganéite-containing sediment samples (samples TMM9 and TMM10 in the litholog) and the position of akaganéite with low magnetic susceptibility below the Ir anomaly in the litholog.

taxa (Figure 7). This unit also consists of high abundances of peridinioid taxa. In Unit 3 and Unit 4, only a few dinocysts are present, revealing low productivity, well-ventilated conditions or both. These intervals also consist of high abundances of charcoal, indicating the prevalence of highly oxygenated conditions.

4.4 | Magnetic polarity stratigraphy

The above analysis and the field information helped in the selection of the palaeomagnetic samples, as the majority of them indicates SSD enrichment with mixed mineralogy. The NRM of the samples is moderate to weak, with intensities for the specimens ranging from 1.02 to 68.5 $\times$ 10^{-4} A/m. The Königsberger ratio 'Q' values for the specimens show a very broad range varying from 0.1 to 6.6. Only the specimens with *Q*-ratio values of more than 0.5 to 1 that indicate the presence of stable remanence are selected for subsequent demagnetization (Königsberger, 1938). Specimens with a lower Q-ratio and inconsistent demagnetization behaviour are not used to generate polarity stratigraphy.

Both thermal (TD) and alternating field (AFD) demagnetization techniques are applied. However, we find that AFD results better than TD with low noise in vector migration and higher consistency around the characteristic remanence (ChRM). This is because the magnetic mineralogy for the majority of rock samples is dominantly ferrimagnetic in nature. The TD results for samples that show an increase in susceptibility at higher temperatures indicate the acquisition of a spurious direction by mineral alteration, and those showing highly scattered vector migration paths are rejected. The primary and secondary components of magnetization are identified by principal component analysis (PCA) for each specimen using Fisherian statistics (Fisher, 1953) (Figures 8–10). In the demagnetization steps with <12.5–25 mT field of AFD and <200–250°C for TD, a soft component is removed having direction near the present-day field. For the AFD results, the majority of the samples display stable components in a wide range between 50–70 mT and 120–160 mT (Figures 8 and 9). For TD, the stable magnetization component with an unblocking temperature in the interval between 275–300°C and 375–400°C is isolated (Figure 10), which also suggests Ti-magnetite and magnetite as the primary remanence carriers. Few samples also revealed a higher

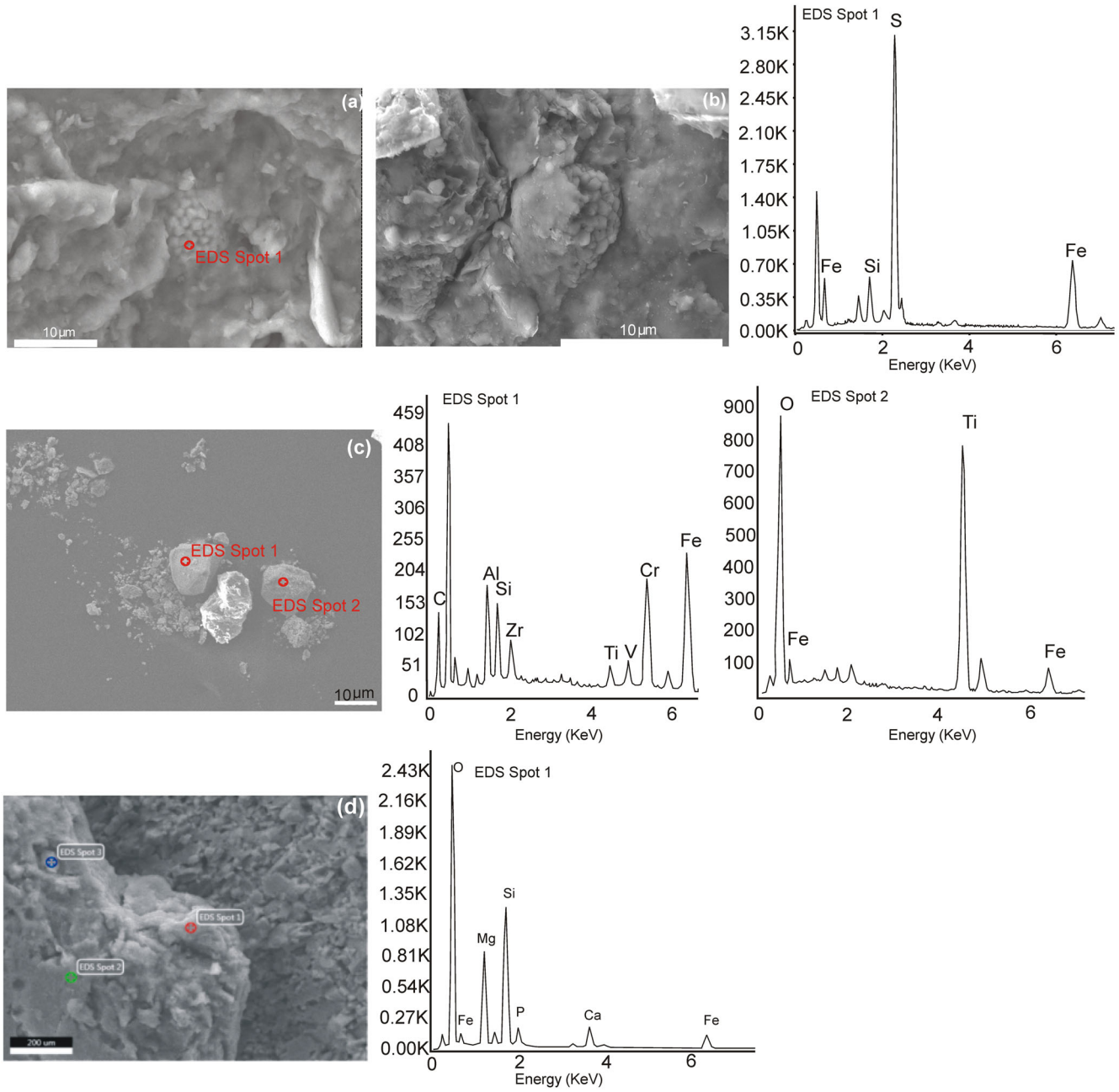

FIGURE 6 Scanning electron microscopy images of representative samples showing (a, b). The presence of framboidal pyrite from the Ir-rich bed (c). Elements such as Cr, V and Ti from the magnetic grain extracts (d). The presence of P in the sediment samples of the Ir-rich bed.

unblocking temperature component between 375 and 525°C. The stable component, also referred to as characteristic remanence magnetization (ChRM), has either normal or reverse polarity with southerly declinations in bedding-corrected coordinates. The declination (*D*), inclination (*I*), VGP latitude and longitude of the samples are given in Table 1.

The ChRM direction for the samples showing normal polarity are combined to form a cluster as well as those showing reverse polarity are also combined to form a separate cluster reveal a mean direction of $D = 351.1°$, $I = -26°$ with $a_{95} = 11.8$ and $K = 9.5$ (after tilt correction) for normal polarity cluster of samples and $D = 169.3°$, $I = 21°$ with $a_{95} = 12.1$ and $K = 7.5$ (after tilt correction) for reverse polarity with angular separation of 174.7° ± 10.4° (Figure 11).

The VGP latitudes are calculated using the mean directions for each sample and plotted against the measured litho-column of the USR section to reconstruct the local magnetic polarity stratigraphy (Figure 12). The positive and negative values of the VGP latitude define normal and reverse polarity events of the geomagnetic field, respectively. These events are correlated with Geomagnetic Polarity Time Scale (GPTS) of Gradstein (2012). The bed containing the Ir-rich layer is considered the datum plane for the matching of the local polarity pattern with the GPTS. The present study is based on

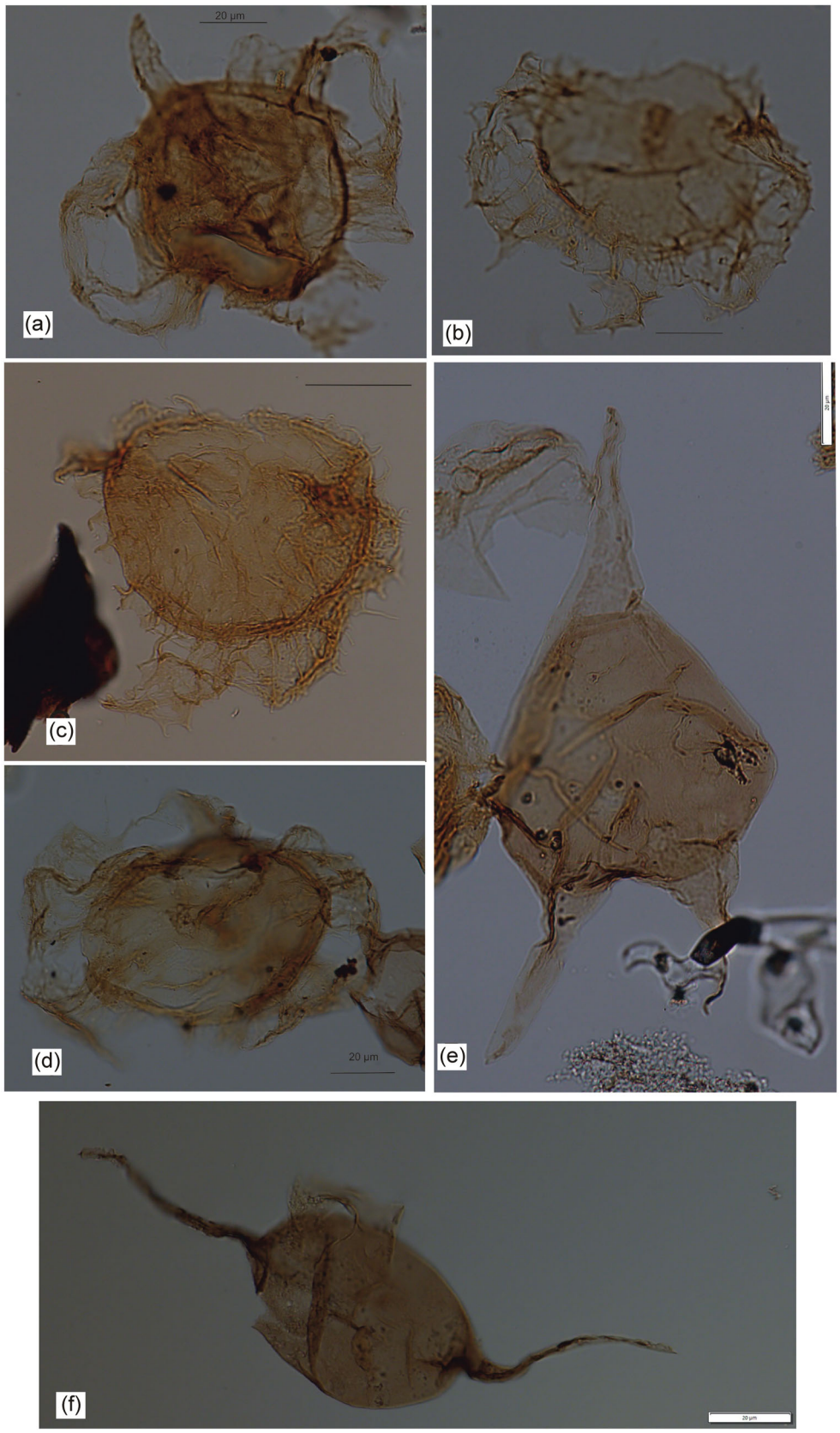

FIGURE 7 The assemblage of dinoflagellate cysts from Unit 2: (a, d) *Disphaerogena carposphaerropsis*; (b, c) *Glaphyrocysta* sp.; (e) *Cerodinium* sp.; (f) *Paleocystodinium* sp.

a limited number of samples due to poor sample recovery from laminated shale beds as well as poor recovery of specimens from single cores of such litho units; therefore, only 52% of the total 331 specimens can be used to generate the result. Many samples are not included in the study due to large scatter and low statistical significance, and others are rejected due to inconsistent

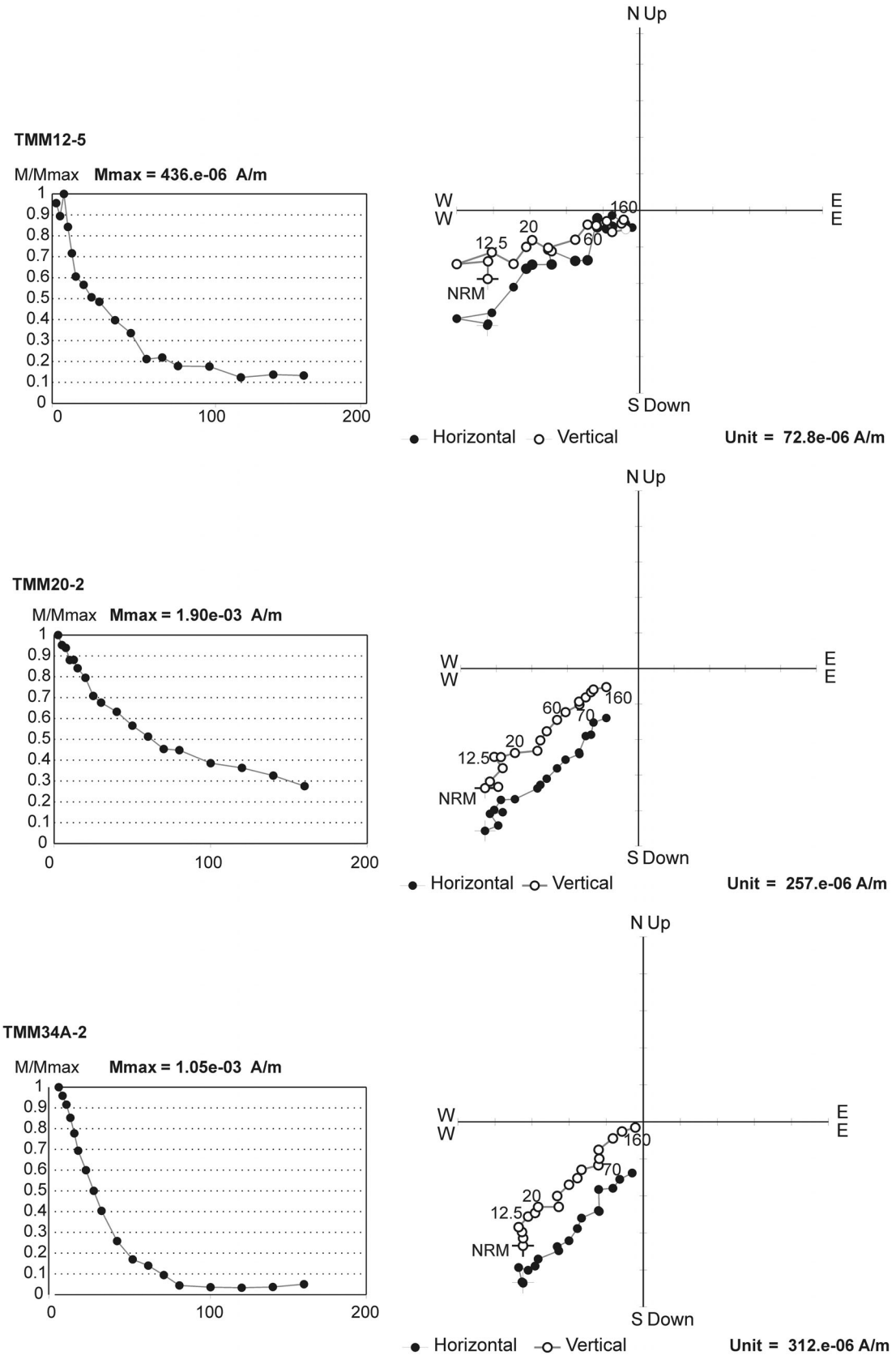

FIGURE 8 Zijderveld diagram and intensity plot during alternating field in mT (AF) demagnetization for tilt corrected specimens TMM12-5, TMM20-2 and TMM34A-2.

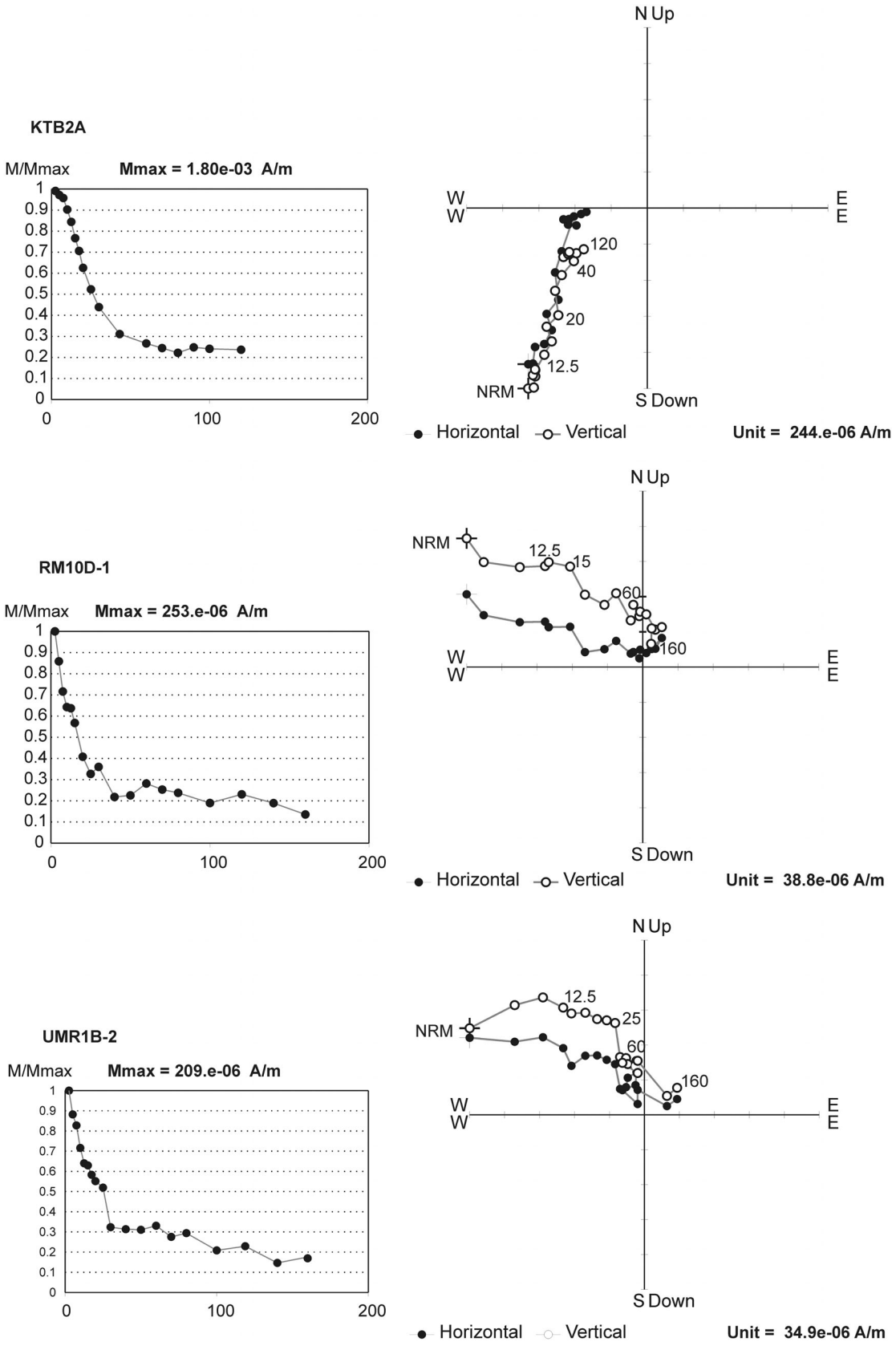

FIGURE 9 Ziderveld diagram and intensity plot during alternating field in mT (AF) demagnetization for tilt corrected specimens KTB2A, RM10-D1 and UMR10B.

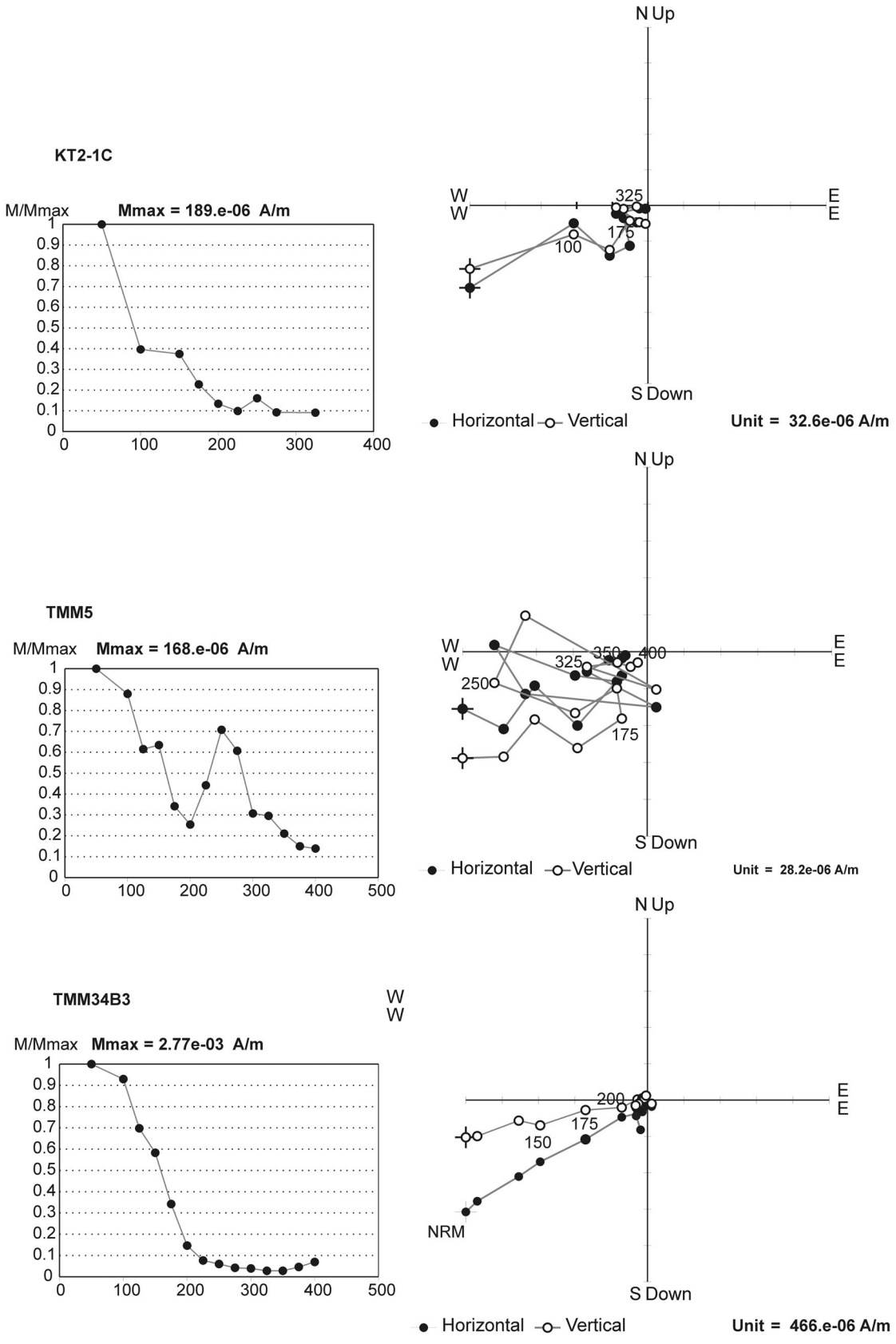

FIGURE 10 Ziderveld diagram and intensity plot during thermal demagnetization in degree Celsius (TD) for tilt corrected specimens KT2-1C, TMM5 and TMM34B-3.

TABLE 1 Values of declination, inclination and virtual geomagnetic poles (VGP) of the sediment sequence from Um Sonryngkew River section of south Shillong Plateau.

Sample	Mean *D* uncorr	Mean *I* uncorr	Mean *D* corr	Mean *I* corr	VGP latitude	VGP longitude
TMM2	195.9	55.5	185.9	36.7	−44.2	83.3
TMM5	174.1	45.6	165.7	15.4	−54.3	115.8
TMM9	138.6	48.4	142.2	13.8	−41.2	145
KTB2	149.7	47.6	153.7	33.3	−39.8	124.2
KT2	249.9	40.7	238.3	36.5	−17.5	34.2
TMM12	190.6	49.9	168.5	25.7	−49.9	108.5
TMM16	209.8	49.8	183.3	43.7	−39.4	87.1
TMM19	168.2	40.7	167.5	15.7	−54.8	112.8
TMM20	221.6	12.7	218.9	4.2	−43.6	31
TMM21	197.1	72.5	162.4	58.9	−23.3	105.7
TMM22	193.6	41.6	181.1	23.7	−52.6	89.2
TMM23	196.7	53.5	176.9	35.9	−45	95.1
TMM24	178.1	51.2	160	29.1	−45	118.8
TMM25	164.1	39.8	158.7	16.8	−50.5	125.4
TMM27	198.4	13.3	194.9	4.4	−59.2	60.9
TMM28	180.8	39.9	178.5	14.3	−57.7	93.8
TMM29	190.9	26.3	188.7	2.7	−62.3	72
TMM30	131.3	19.9	132.6	−6.9	−39.6	163.6
TMM31	159.1	35.3	158.4	8.4	−54	129.7
TMM32	111.5	14.6	112.5	−3.1	−21	172.6
TMM33	146.7	19.4	146.3	−0.5	−49.1	148.9
TMM34	174.4	24	171.4	12.1	−57.8	107.2
UMR1	356.7	−15	340.4	−45.8	34.5	292.2
UMR2	7.1	4.4	11.7	−23.3	51.1	252.6
UMR3	351.8	−28	333.1	−46.8	31	298.8
UMR4	338.3	−31.6	336.3	−4.2	54.5	314.7
UMR5	12.4	−20.6	8.6	−0.8	63.3	251.6
UMR6	329	−40.1	329.2	−11.1	47.2	319.6
UMR7	42	−24.1	34.1	−11.6	44.7	219.3
UMR9	346.8	−31.6	344.3	−2.6	59.6	303.3
UMR10	3.7	−59	348.1	−40.9	40.2	285.3
UMR12	351.9	−32.4	347.5	−4.1	60.4	296.9
UMR15	16.6	−32.7	6	−12.3	58.2	259.6
UMR16	7.7	−54.6	349.9	−30.7	47.3	285.4
UMR17	324.9	−9.2	312.9	−39.2	24.3	319.1
UMR18	329.8	−12.4	320.8	−39	29.5	313.3
RM1	356	−18.1	347.1	−44.7	37.2	285.5
RM5	293.7	−81.5	329.6	−53.7	24.1	298.3
RM9	33.6	−26.2	22.9	−14.8	50.6	233.6
RM10	20	−33.5	8.6	−15.6	56	255.6

Note: corr, tilt corrected; *D*, declination; *I*, inclination, uncorr, uncorrected.

demagnetization behaviour. Samples with at least three specimens are only used to define the polarity intervals. The inclination data and VGP are considered to develop the magnetostratigraphy of the section (Figure 12).

5 | DISCUSSION

The USR section of Meghalaya is one of the most complete Cretaceous-Paleogene marine sedimentary sequences from India.

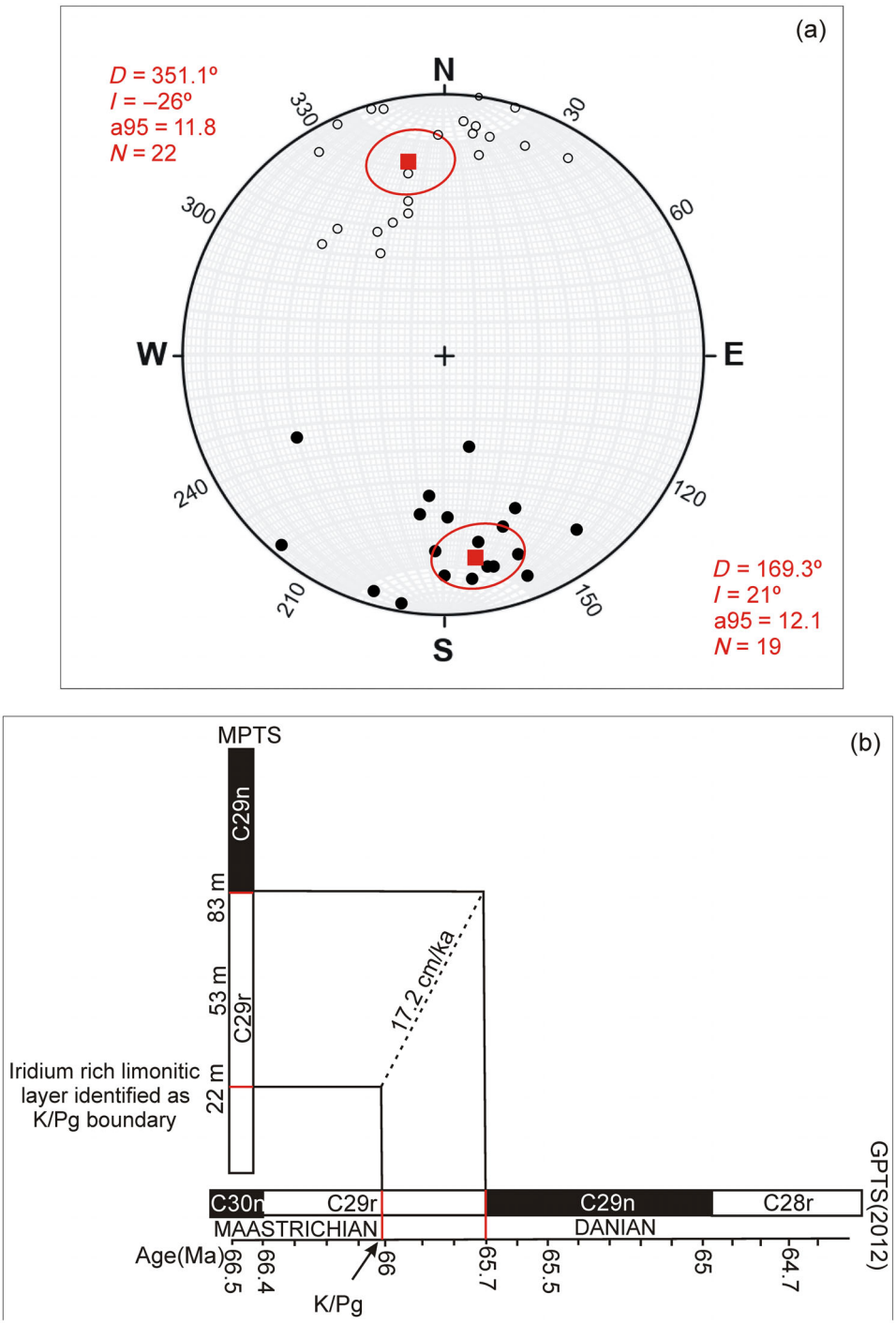

FIGURE 11 (a) Equal area projection of the mean palaeomagnetic directions obtained for normal and reverse polarity obtained from the Um Sohrynkew sedimentary sequence with 95% confidence cones. Closed and open symbols indicate positive and negative inclinations, respectively. (b) Average sediment accumulation rate for the 61 m portion of the sequence above the Ir anomaly.

Many significant studies, including litho- and biostratigraphic zonations of the strata (Bhattacharya & Bhattacharya, 1981; Biswas, 1962; Dalabehera et al., 2021; Garg et al., 2006; Nandi, 1990; Oldham, 1859; Pandey, 1981, 1990) and geochemical analysis (N. Bhandari et al., 1987; N. Bhandari et al., 1994; Gertsch et al., 2011; Pal et al., 2015; Pal & Shrivastava, 2020; Sial et al., 2016), have been conducted to temporally constrain the K-Pg event and decipher palaeoenvironmental/climatic conditions. The present study is the first report of magnetic polarity and magnetic mineralogy from this section.

The rock magnetic signatures have revealed the predominance of ferrimagnetic minerals such as magnetite/maghemite (and Ti-magnetite) and a mixed mineralogy (ferri and antiferromagnetic minerals represented by haematite and goethite) in many intervals. The ferrimagnetic phases have dominated both the rock magnetic signatures and palaeomagnetic remanances. The rock magnetic signatures show that the abundance of SSD grains provides stable remanence. Magnetic polarity analysis encounters two magnetozones (1 Reverse and 1 Normal). The Ir anomaly layer present in the sequence is used as the age marker to facilitate correlation with the GPTS. Unit 1, Unit 2 with

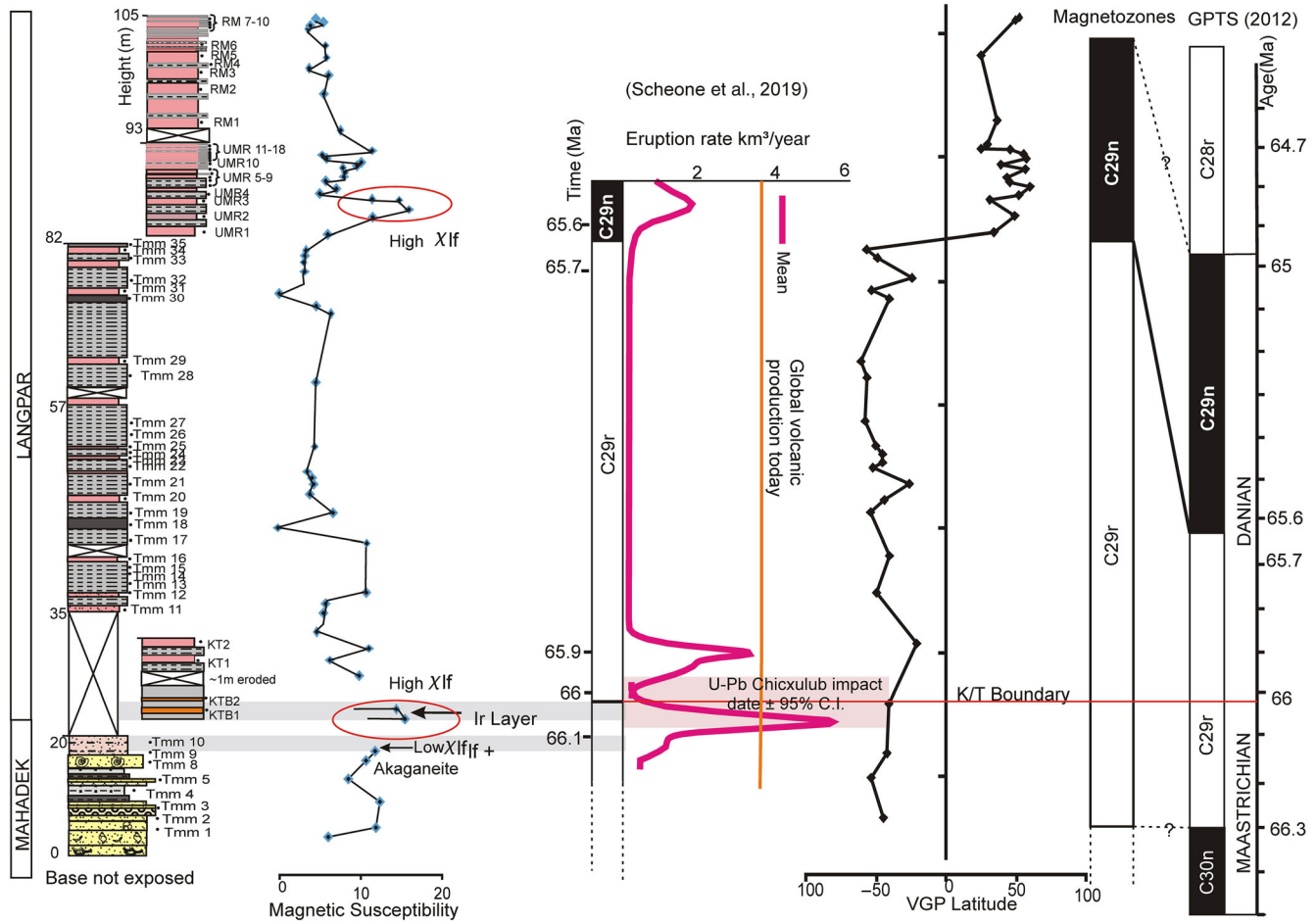

FIGURE 12 Virtual geomagnetic poles latitudes, magnetic susceptibility, Deccan eruption rate and magnetic polarity correlation to Geomagnetic Polarity Time Scale (Gradstein, 2012) of Um Sohrynkew River section, Meghalaya.

the Ir layer and Unit 3 falls in the reverse magnetic zone that can be correlated with C29r (Figure 12). This is followed by the normal polarity for Units 4–5 correlated with C29n. The first report of palaeomagnetic data from the Khasi group (Jadukata and Mahadek formations) of sediments is provided by Rao Poornachandra et al. (2000), indicating dominantly reverse magnetization during Khasi Group sedimentation and suggesting that the Mahadek Formation may overlap with the Early Paleocene. However, the present study indicates that Mahadek sedimentation continues not further than the Upper Maastrichian in conformity with stratigraphic age indicated by palynostratigraphy and marine invertebrate fauna such as *Stygmatopygus* of Upper Cretaceous age reported from the top part of the Mahadek sandstone (Bhattacharyya & Bhattacharya, 1981; Mukherjee, 2012; Nandi, 1990). The antipodal mean directions (Figure 11) of the normal and reverse polarity samples indicate that the ChRM is of primary origin (Appel et al., 1991). Therefore, the K-Pg boundary in the USR section can be taken as a standard in the region, and more detailed studies, such as paleointensity, may be conducted in the future.

In the present study, the Ir anomaly layer of N. Bhandari et al. (1994) is considered as the K-Pg boundary as it falls with the C29r and conforms to the carbon isotope and planktic forminiferal biostratigraphy of Gertsch et al. (2011). The lithological change at the onset of the Ir-based K-Pg boundary from the majority of sandstones to mudstones depicts a rapid change in depositional environment from continental-shelfal to deep shelf conditions with a continuous sedimentation. The C29r/C29n of the 65.688 Ma event occurs at 61 m above the Ir layer considered to be 66.043 Ma (the K-Pg boundary). This implies that the 61 m interval represents a time duration of 0.355 Ma (355 Ka) with an estimated rate of sedimentation of approximately 17.2 cm/ka (Figure 11b).

5.1 | Mineralogical and rock magnetic signatures along the K-Pg boundary in the USR section

Many earlier studies on different sedimentary sequences worldwide have inferred that rock magnetic signals, particularly magnetic susceptibility (χlf), are a marker for the K-Pg boundary interval (Abrajevitch et al., 2015; Ellwood et al., 2003; Hansen et al., 1993). Low magnetic susceptibility in association with the mineral akaganéite is considered as an independent marker for the K-Pg boundary, and its occurrence is suggested to be a global-scale phenomenon (Font et al., 2011).

Akaganéite is a Cl-bearing iron (hydro) oxide, and the association of Cl with iron oxides is a very unusual occurrence in a sedimentary environment. Its presence in a sedimentary sequence is attributed to terrestrial volcanism in association with the Deccan eruption (Font et al., 2011, 2017). Self et al. (2008) quantified and suggested that enormous amounts of S and Cl were released during Deccan volcanism. Approximately 70%–80% of the eruption took place during Phase 2 of Deccan volcanism (Renne et al., 2015), encompassing the K-Pg boundary interval. Low magnetic susceptibility with akaganéite is reported from the Biddart, Gubbio and Zumaia sections, which are approximately 8000 km away from the Deccan volcanic province (Font et al., 2016, 2018); thus, sites proximal to the DVP, such as the present study location, may hold much higher potential to record its presence and can contribute to constraining the K-Pg interval and interpreting contemporary palaeoenvironmental conditions.

For Biddart and Gubbio, a clear low magnetic susceptibility occurs below the Cretaceous-Paleogene boundary (K-Pg), and a typical high susceptibility representing a clay layer is seen just above the K-Pg (Ellwood et al., 2003; Font et al., 2016). Akaganéite is observed in a 50 cm thick interval located 5 cm below K-Pg for Gubbio and Biddart. However, for the Zumaia section, a gradual decrease in susceptibility for 1.5 m is seen that encompasses the K-Pg, with no high susceptibility peak and akaganéite is observed within a 1 m thick interval spanning K-Pg within the low susceptibility zone. Font et al. (2011) explained that this low susceptibility resulting from detrital magnetite dissolution due to acidic environmental conditions driven by acid rain is compatible with the timing of Deccan volcanism. In the present study, a peak in magnetic susceptibility (Peak-1) is observed for Unit 2 in the limonitic clay bed containing Ir anomaly (Figure 5) and the mineral akaganéite identified with the help of SEM–EDS is observed in the low magnetic susceptibility zone underlying the Ir layer (Figure 5). This interval containing Ir also shows the presence of framboidal pyrite of <10 μm at the K-Pg boundary that indicates dysoxic conditions (Wignall et al., 2010), which is also corroborated by geochemical analysis of the Um Sohryngkew section by Gretsch et al. (Gertsch et al., 2011). Occurrence of pyrite framboids has also been reported from the Ir layer in this section by Dalabehera et al. (2021). Sial et al. (2016, 2019) studied mercury isotope (considered as a good indicator of volcanism) from a different K-Pg section in Meghalaya and suggested indication of Deccan phase 2 from interval below K-Pg boundary and after carbon dioxide, sulfuric aerosol and other toxic agents reached critical threshold. This observation of Sial et al. (2019) supports the occurrence of akaganéite below the K-Pg boundary from the present section as well. Unit 2 also consists of high abundances of peridinioid taxa, as seen from dinocyst analysis. The heterotrophic nature of Peridinoides shows affinity for conditions like high runoff, turbidity and low light. In addition, peridinoid cysts are dominant in unstable conditions and sensitive to redox condition (Uddandam et al., 2018; Zonneveld et al., 2013). Thus, the high abundance of peridinoid reveals terrestrial influx and low oxygenated conditions in the late Maastrichtian. Recently, Ghoshmaulik et al. (2023) reported high rainfall based on triple oxygen isotopes during the K-Pg boundary from intertrappean fossil woods from Central India. The intensified rainfall during the K-Pg interval could have resulted in high terrestrial nutrient and dinocyst preservation, including peridinioid cysts.

Akaganéite precipitation requires an acidic oxidizing hyperchlorinated environment or acidic-sulfidic settings (Bibi et al., 2011; Carter et al., 2015; Font et al., 2018). Rock magnetic analysis also shows that the interval (below K-Pg) of the Um Sohryngkew section is coincident with high antiferromagnetic and decreased magnetite content, suggesting an oxidizing condition. Where as a dysoxic condition is noted for the K-Pg boundary hosting the Ir layer. These observations confirm that during the K-Pg interval, a highly stressed environmental condition with a fluctuating redox state occurred. Thus, the association of the akaganéite within the low susceptibility interval below the Ir layer suggests a signature of Deccan volcanism. On the other hand, the high susceptibility within the Ir layer (highest in the entire section) can be attributed to the highest SP fraction (very high χfd%) in the section can be related to the aeorosol origin of the ferrimagnets. The aerosol generation and loading can be related to either (i) volcanism or (ii) the meteoritic impact. Interestingly, Ponte (2013) has also reported similar high χfd% coinciding with a peak of high magnetic susceptibility on a red clay level from K-Pg section of Podgawan from Deccan Trap region of India. The section also showed various populations of magnetite with various amount of titanium similar to the present study. Ponte (2013) inferred these observations to be resulted from severe weathering and stressed paleo-environmental conditions during the Deccan phase-2. The high susceptibility and χfd % depicting the SP fraction need to be studied in detail using advanced spectroscopic and rock magnetic methods to understand their origin. The present findings thus suggest the potential for the Um Sohryngkew section to identify relative position of impact and Deccan Phase 2 that can help to resolve the age issue, related extinction event and correlate with other K-Pg sections around the world.

6 | CONCLUSIONS

In the present study, rock magnetic and palaeomagnetic signatures are utilized to derive new data and inferences from the USR section of Meghalaya, which is widely referred to host the K-Pg boundary in India. The main inferences are as follows:

1. According to this study, the C29r/29n (65.688 Ma) reversal occurs at 61 m above the Ir layer, which is considered 66.043 Ma (K-Pg boundary), and the 61 m interval represents a time duration of 0.355 Ma (355 Ka) with an estimated rate of sedimentation of 17.2 cm/ka. This laid the groundwork for future studies in developing more comprehensive palaeomagnetic-paleointensity analysis along with magnetostratigraphy to develop robust correlation of the K-Pg boundary from this region.
2. Furthermore, the magnetic susceptibility anomaly (Peak-1) matching the Ir layer depicts significant aerosol input as inferred from the high SP concentration (high χfd%). The aerosols may be sourced from volcanism or meteoritic impacts. This study also reports the presence of akaganéite from the K-Pg section of Um

Sohryngkew matching with a low magnetic susceptibility interval below the K-Pg boundary and suggest signature of Deccan volcanism phase 2 from the section. Detailed study of akaganéite needs further research.

3. The findings confirm the stressful palaeo-environmental conditions took place during the K-Pg interval and shift from acidic oxidizing (akaganéite + low χlf + antiferromagnetic components) to reducing/dysoxic and increased influx/turbidity conditions (high χlf + very high χfd% + fraimboidal pyrites + peridinoides dinoflagellate cysts).

AUTHOR CONTRIBUTIONS

D.N. and V.P. conceived and designed the study. D.N., P.R.U., A.C. conducted field work. D.N. and S.P.S. performed palaeomagnetic, rock magnetic and SEM laboratory investigations. P.R.U. performed dinoflagellate cyst and A.C. performed sedimentological studies. D.N., S.P.S, S.J.S. and B.P. analysed the data. D.N. prepared the manuscript. All authors contributed to the discussion and approved the final proof.

ACKNOWLEDGEMENTS

The authors are thankful to the Head, Department of Geology, Savitribai Phule Pune University for encouragement and support permission to avail Rock Magnetic Lab. The authors are also grateful to the Director, Birbal Sahni Institute of Palaeosciences, Lucknow, India for support and using SAIF facility of BSIP for the research work. Debarati Nag is thankful to the Director BSIP for providing BSRA fellowship. Dr. Sabyasachi Mandal (Scientist B, BSIP) is acknowledged for his fruitful discussions during the field work.

DATA AVAILABILITY STATEMENT

Data will be available upon request.

ORCID

Binita Phartiyal https://orcid.org/0000-0003-3086-8735

REFERENCES

Abrajevitch, A., Font, E., Florindo, F., & Roberts, A. P. (2015). Asteroid impact vs. Deccan eruptions: The origin of low magnetic susceptibility beds below the Cretaceous Paleogene boundary revisited. *Earth and Planetary Science Letters*, *430*, 209–223.

Ali, M. A., & Duarah, B. P. (2022). Tectono-stratigraphic evolution of Shillong Plateau, North East India through the Permian-Eocene window. *Geological Journal*, *57*, 5127–5148.

Alvarez, L. W. (1980). Extraterrestrial cause for the Cretaceous-Tertiary extinction-experimental results and theoretical interpretation. *Science*, *208*, 1095–1108.

Alvarez, W., Kauffman, E. G., Surlyk, F., Alvarez, L. W., Asaro, F., & Michel, H. V. (1984). Impact theory of mass extinctions and the invertebrate fossil record. *Science*, *223*, 1135–1141.

Appel, E., Rösler, W., & Corvinus, G. (1991). Magnetostratigraphy of the Miocene-Pleistocene Surai Khola Siwaliks in West Nepal. *Geophysical Journal International*, *105*, 191–198.

Bernaola, G., Baceta, J. I., Payros, A., Orue-Etxebarria, X., & Apellaniz, E. (Eds.). (2006). *The Paleocene and lower Eocene of the Zumaia section (Basque Basin). Climate and biota of the Early Paleogene 2006*. Post Conference Field Trip Guidebook. Bilbao.

Bhandari, N., Gupta, M., Pandey, J., & Shukla, P. M. (1994). Chemical profiles in K/T boundary section of Meghalaya, India: Cometary, asteroidal or volcanic. *Chemical Geology*, *113*, 45–60.

Bhandari, N., Shukla, P. N., & Castagnoli, G. C. (1993). Geochemistry of some K/T sections in India. *Palaeogeography, Palaeoclimatology, Palaeoecology*, *104*, 199–211.

Bhandari, N., Shukla, P. N., & Pandey, J. (1987). Iridium enrichment at Cretaceous-Tertiary boundary in Meghalaya. *Current Science*, *56*, 1003–1005.

Bhattacharyya, A., & Bhattacharya, U. (1981). Biostratigraphic zonation of the Upper Cretaceous Formations of Khasi and Jaintia Hills, Meghalaya. *Palaeontological Society of India*, *26*, 26–31.

Bibi, I., Singh, B., & Silvester, E. (2011). Akaganeite (beta-FeOOH) precipitation in in-land acid sulfate soils of south–western, New South Wales (NSW), Australia. *Geochimica et Cosmochimica Acta*, *75*, 6429–6438.

Biswas, B. (1962). Stratigraphy of the Mahadeo, Langpar, Cherra and Tura Formations, Assam, India. *Bulletin of the Geological Mining and Metallurgical Society of India*, *25*, 1–25.

Cande, S. C., & Kent, D. V. (1995). Revised calibration of the geomagnetic polarity time scale for the late Cretaceous and Cenozoic. *Journal of Geophysical Research*, *100*, 6093–6095.

Carter, J., Viviano-Beck, C., Loizeau, D., Bishop, J., & Le Deit, L. (2015). Orbital detection and implications of Akaganeite on Mars. *Icarus*, *253*, 296–310.

Chadima, M., & Hrouda, F. (2006). Remasoft 3.0–a user friendly paleomagnetic data browser and analyzer. *Travaux Geophysiques*, *27*, 20–21.

Chakraborty, A., & Bakshi, S. (1972). Stratigraphy of the Cretaceous—Tertiary sedimentary sequence, southwest of Shillong plateau. *Quarterly Journal of the Geological, Mining and Metallurgical Society of India*, *44*, 109–127.

Chenet, A.-L., Courtillot, V., Fluteau, F., Gérard, M., Quidelleur, X., Khadri, S. F. R., Subbarao, K. V., & Thordarson, T. (2009). Determination of rapid Deccan eruptions across the Cretaceous-Tertiary boundary using paleomagnetic secular variation: 2. Constraints from analysis of eight new sections and synthesis for a 3500-m-thick composite section. *Journal of Geophysical Research*, *114*, B06103.

Courtillot, V., Féraud, G., Maluski, H., Vandamme, D., Moreau, M. G., & Besse, J. (1988). Deccan flood basalts and the Cretaceous/Tertiary boundary. *Nature*, *333*, 843–846.

Dalabehera, L., Iangrai, B., & Mukherjee, D. (2021). Stratigraphy and faunal assemblages of the Upper Cretaceous sediments of Meghalaya shelf: Palaeoenvironmental implications. *Journal Geological Society of India*, *97*, 1033–1048.

Dannemann, S., Appel, E., Rösler, W., Neumann, U., Liebke, U., & Nag, D. (2022). Palaeomagnetic indication for India–Asia collision at 12° N and maximum 810 km greater India extent in the western suture zone. *Geophysical Journal International*, *229*, 1193–1211.

Deng, C., Zhu, R., Verosub, K. L., Singer, M. J., & Vidic, N. J. (2004). Mineral magnetic properties of loess/paleosol couplets of the Central Loess Plateau of China over the last 1.2 Myr. *Journal of Geophysical Research*, *109*, B01103.

Deng, C. L., Zhu, R. X., Jackson, M. J., Verosub, K. L., & Singer, M. J. (2001). Variability of the temperature-dependent susceptibility of the Holocene eolian deposits in the Chinese Loess Plateau: A pedogenesis indicator. *Physics and Chemistry of the Earth, Part A: Solid Earth and Geodesy*, *26*, 873–878.

Desikachar, S. V. (1974). A review of the tectonic and geological history of eastern India in terms of plate tectonic theory. *Journal Geological Society of India*, *15*, 137–149.

Devi, N. R., & Sarma, K. P. (2010). Strain analysis and stratigraphic status of Nongkhya, Sumer and Mawmaram Conglomerates of Shillong basin, Meghalaya, India. *Journal of Earth System Science*, *119*, 161–174.

Ellwood, B. B., MacDonald, W. D., Wheeler, C., & Benoist, S. L. (2003). The K-T boundary in Oman: Identified using magnetic susceptibility field measurements with geochemical confirmation. *Earth and Planetary Science Letters*, *206*, 529–540.

England, P. C., & Bilham, R. (2015). The Shillong Plateau and the great 1897 Assam earthquake. *Tectonics*, *34*, 1792–1812.

Enkin, R., Wuolle, K., Mccann, C., Carretero, M., Voroney, M., Baylis, T., Morton, K., Jaycock, D., Baker, J., & Beran, L. (2003). *PMGSC–paleomagnetism data analysis, ver. 4.2*. Geological Survey of Canada.

Evans, P. (1964). The tectonic framework of Assam. *Journal Geological Society of India*, *5*, 88–96.

Fisher, R. A. (1953). Dispersion on a sphere. *Proceedings of the Royal Society of London Series A: Mathematical and Physical Sciences*, *217*, 295–305.

Font, E., Adatte, T., Andrade, M., Keller, G., Bitchong, A. M., Carvallo, C., Ferreira, J., Diogo, Z., & Mirão, J. (2018). Deccan volcanism induced high-stress environment during the Cretaceous–Paleogene transition at Zumaia, Spain: Evidence from magnetic, mineralogical and biostratigraphic records. *Earth and Planetary Science Letters*, *484*, 53–66.

Font, E., Adatte, T., Sial, A. N., Drude de Lacerda, L., Keller, G., & Punekar, J. (2016). Mercury anomaly, Deccan volcanism, and the end-Cretaceous mass extinction. *Geology*, *44*, 171–174.

Font, E., & Bond, D. P. (2021). Volcanism and mass extinction. In D. Alderton & S. A. Elias (Eds.), *Encyclopedia of geology* (pp. 569–606). Academic Press.

Font, E., Carlut, J., Remazeilles, C., Mather, T. A., Nedelec, A., Mirao, J., & Casale, S. (2017). End-Cretaceous Akaganeite as a mineral marker of Deccan volcanism in the sedimentary record. *Scientific Reports*, *7*, 11453.

Font, E., Nedelec, A., Ellwood, B. B., Mirao, J., & Silva, P. F. (2011). A new sedimentary benchmark for the Deccan Traps volcanism? *Geophysical Research Letters*, *38*, L24309.

Garg, R., & Jain, K. P. (1995). Significance of the terminal Cretaceous calcareous nannofossil marker Micula prinsii at the Cretaceous–Tertiary boundary in Um Sohryngkew River section, Meghalaya, India. *Current Science*, *69*, 1012–1017.

Garg, R., Khowaja, A., & Prasad, V. (2006). Significant dinoflagellate cyst biohorizons in the Upper Cretaceous-Palaeocene succession of the Khasi Hills. *Meghalaya Journal Geological Society of India*, *67*, 737–747.

Gertsch, B., Keller, G., Adatte, T., Garg, R., Prasad, V., Berner, Z., & Fleitmann, D. (2011). Environmental effects of Deccan volcanism across the Cretaceous–Tertiary transition in Meghalaya, India. *Earth and Planetary Science Letters*, *310*, 272–285.

Ghosh, A. M. N. (1940). Stratigraphical position of the Cherra sandstone, Assam. *General Report of the Geological Survey of India*, *75*, 17–18.

Ghosh, S. K., Chakravorty, S., Bhalla, J. K., Paul, D. K., Sarkar, A., Bishui, P. K., & Gupta, S. N. (1994). New Rb–Sr isotopic ages and geochemistry of granitoids from Meghalaya and their significance in middle to late Proterozoic crustal evolution. *Indian Minerals*, *48*, 33–44.

Ghoshmaulik, S., Bhattacharya, S. K., Hazra, M., Roy, P., Khan, M. A., Liang, M., Iizuka, Y., Hsiao, S., Lee, D., & Sarkar, A. (2023). Triple oxygen isotopes in intertrappean fossil woods: Evidence of higher tropical rainfall during Deccan volcanism. *Chemical Geology*, *634*, 121599.

Govin, G., Najman, Y., Copley, A., Millar, I., van der Beek, P., Huyghe, P., Grujic, D., & Davenport, J. (2018). Timing and mechanism of the rise of the Shillong Plateau in the Himalayan foreland. *Geology*, *46*, 279–282.

Gradstein, F. M. (Ed.). (2012). *The geologic time scale 2012* (Vol. 45, pp. 171–188). Elsevier.

GSI. (2009). *Geological survey of India* (Vol. 30). Miscellaneous Publication. Part IV, Vol. 2(ii).

Hansen, H. J., Rasmussen, K. L., Qingsheng, L., Benjamini, C., Walaszczyk, I., Gwozdz, R., & Stage, M. (1993). Correlation of marine and terrestrial Upper Cretaceous sediments by their magnetic susceptibility. *Bulletin of the Geological Society of Denmark*, *40*, 175–184.

Keller, G., Adatte, T., Stinnesbeck, W., Stüben, D., Berner, Z., Kramar, U., & Harting, M. (2004). More evidence that the Chicxulub impact predates the K/T mass extinction. *Meteorites and Planetary Science*, *39*, 1127–1144.

Keller, G., Stinnesbeck, W., Adatte, T., & Stüben, D. (2003). Multiple impacts across the Cretaceous Tertiary boundary. *Earth Science Reviews*, *62*, 327–363.

Kirschvink, J. L. (1980). The least-squares line and plane and the analysis of palaeomagnetic data. *Geophysical Journal International*, *62*, 699–718.

Königsberger, J. (1938). Natural residual magnetism of eruptive rocks. *Terrestrial Magnetism and Atmospheric Electricity*, *43*, 299–320.

Lahiri, T. C., Sen, M. K., Raychaudhuri, A. K., & Acharyya, S. K. (1988). Observations on Cretaceous/Tertiary boundary and reported iridium enrichment, Khasi Hills, Meghalaya. *Current Science*, *57*, 1335–1336.

Liu, Q., Deng, C., Yu, Y., Torrent, J., Jackson, M. J., & Banerjee, S. K. (2005). Temperature dependence of magnetic susceptibility in an argon environment: Implications for pedogenesis of Chinese loess/palaeosols. *Geophysical Journal*, *161*, 102–112.

Liu, Q. S., Roberts, A. P., Torrent, J., Horng, C. S., & Larrasoaña, J. C. (2007). What do the HIRM and S-ratio really measure in environmental magnetism? *Geochemistry Geophysics Geosystems*, *8*, Q09011.

Maher, B. A. (1988). Magnetic properties of some synthetic sub-micron magnetites. *Geophysical Journal International*, *94*, 83–96.

Medlicott, H. B. (1869). Geological sketch of the Shillong plateau in north eastern Bengal. *Memoirs of the Geological Survey of India*, *7*, 1–57.

Mishra, U. K., & Sen, S. (2001). Dinosaur bones from Meghalaya. *Current Science*, *80*, 1053–1056.

Mitra, S. K. (1998). *Structure, sulphidemineralisation and age of the Shillong group of rocks (abstract), Meghalaya*. S.K. Krishnan Centenary Commemorative National Seminar, 1–2 November, Calcutta (pp. 118–119).

Mukherjee, D. (2012). A diverse invertebrate assemblage from the Upper Maastrichtian of Meghalaya and its biogeographic significance. *Indian Journal of Geosciences*, *66*, 233–246.

Mukhopadhyay, S. K. (2008). Planktonic foraminiferal succession in late Cretaceous to early Palaeocene strata in Meghalaya, India. *Lethaia*, *41*, 71–84.

Murthy, M. V. N., Chakraborty, C., & Talukdar, S. C. (1976). Stratigraphic revision of the Cretaceous-Tertiary sediments on the Shillong Plateau. *Records of Geological Survey of India*, *107*, 80–90.

Nagappa, Y. (1959). Foraminiferal biostratigraphy of the cretaceous: Eocene succession in the India-Pakistan-Burma region. *Micropaleontology*, *5*, 145–192.

Nandi, B. (1990). Palynostratigraphy of Upper Cretaceous sediments, Meghalaya, northeastern India. *Review of Palaeobotany and Palynology*, *65*, 119–129.

Oldham, T. (1859). On the geological structure of a portion of the Khasi and Jaintia Hills, Bengal. *Memoirs of the Geological Survey of India*, *1*, 99–210.

Pal, S., & Shrivastava, J. P. (2020). Cretaceous/Palaeogene boundary transition induced lattice defects in illite and kaolinite associated with the Um-Sohryngkew river section, Meghalaya, India. *Solid Earth Sciences*, *5*, 202–222.

Pal, S., Shrivastava, J. P., & Mukhopadhyay, S. K. (2015). Mineral chemistry of clays associated with the late cretaceous-early Palaeogene succession of the Um-Sohryngkew river section of Meghalaya, India: Palaeoenvironmental inferences and K-Pg transition. *Journal Geological Society of India*, *86*, 631–647.

Pandey, J. (1981). Cretaceous foraminifera of um Sohryngkew River section, Meghalaya. *Journal of the Palaeontological Society of India*, *25*, 53–74.

Pandey, J. (1990). Cretaceous/Tertiary boundary, iridium anomaly and foraminifer breaks in the Um Sohryngkew River section. *Current Science*, *59*, 570–575.

Ponte, J. M. N. (2013). *Magnetic mineralogy of Cretaceous-Tertiary sections (Tethys, Iran and India): Links with the Deccan Phase-2* (Dissertation). Universidade De Lisboa (pp. 1–33).

Rao Poornachandra, G. V. S., Rao Mallikarjuna, J., & Bhalla, M. S. (2000). Late Cretaceous sediments of Khasi Group from Meghalaya and their palaeomagnetic implications. *Memoir of Geological Society of India*, *46*, 355–364.

Renne, P. R., Deino, A. L., Hilgen, F. J., Kuiper, K. F., Mark, D. F., Mitchell, W. S., III, Morgan, L. E., Mundil, R., & Smit, J. (2013). Time scales of critical events around the Cretaceous-Paleogene boundary. *Science*, *339*, 684–687.

Renne, P. R., Sprain, C. J., Richards, M. A., Self, S., Vanderkluysen, L., & Pande, K. (2015). State shift in Deccan volcanism at the Cretaceous-Paleogene boundary, possibly induced by impact. *Science*, *350*, 6256–6278.

Schoene, B., Samperton, K. M., Eddy, M. P., Keller, G., Adatte, T., Bowring, S. A., Khadri, S. F., & Gertsch, B. (2015). U-Pb geochronology of the Deccan Traps and relation to the end-Cretaceous mass extinction. *Science*, *347*, 182–184.

Schwertmann, U., & Taylor, R. G. (1989). Iron oxides. In J. B. Dixon, & S. Weed (Eds.), *Minerals in soil environments* (pp. 145–180). Soil Science Society of America.

Self, S., Jay, A. E., Widdowson, M., & Keszthelyi, L. P. (2008). Correlation of the Deccan and Rajahmundry trap lavas: Are these the longest and largest lava flows on Earth? *Journal of Volcanology and Geothermal Research*, *172*, 3–19.

Sial, A. N., Chen, J., Lacerda, L. D., Frei, R., Higgins, J. A., Tewari, V. C., Gaucher, C., Ferreira, V. P., Cirilli, S., Peralta, S., Korte, C., Barbosa, J. A., Pereira, N. S., & Ramos, D. S. (2019). Chemostratigraphy across the Cretaceous-Paleogene (K-Pg) boundary: Testing the impact and volcanism hypotheses. In A. N. Sial, C. Gaucher, M. Ramkumar, & V. P. Ferreira (Eds.), *Chemostratigraphy across major chronological boundaries, geophysical monograph series 240* (pp. 223–257). John Wiley & Sons, Inc.

Sial, A. N., Chen, J., Lacerda, L. D., Frei, R., Tewari, V. C., Pandit, M. K., Gaucher, C., Ferreira, V. P., Cirilli, S., Peralta, S., Korte, C., Barbosa, J. A., & Pereira, N. S. (2016). Mercury enrichments and Hg isotopes in Cretaceous-Paleogene boundary successions: Links to volcanism and palaeoenvironmental impacts. *Cretaceous Research*, *66*, 60–81.

Uddandam, P. R., Prasad, V., Thakur, B., & Manoj, M. C. (2018). *Cristadinium striatiserratum*: A dinoflagellate cyst from the tropical region. *Journal of Palaeontological Society of India*, *63*, 73–80.

Wignall, P. B., Bond, D. P. G., Kuwahara, K., Kakuwa, Y., Newton, R. J., & Poulton, S. W. (2010). An 80 million year oceanic redox history from Permian to Jurassic pelagic sediments of the Mino-Tambaterrane, SW Japan, and the origin of four mass extinctions. *Global and Planetary Change*, *71*, 109–123.

Zijderveld, J. D. A. (1967). A. C. Demagnetization of rocks: Analysis of results. In D. W. Collinson, K. M. Creer, & S. K. Runcorn (Eds.), *Methods in palaeomagnetism* (pp. 254–286). Elsevier.

Zonneveld, K. A. F., Marret, F., Versteegh, G. J. M., Bogus, K., Bouimetarhana, I., Crouch, E., de Vernal, A., Elshanawany, R., Esper, O., Forke, S., Grøsfjeld, K., Henry, M., Holzwarth, U., Bonnet, S., Edwards, L., Kielt, J. F., Kim, S. Y., Ladouceur, S., Ledu, D., … Verleye, T. (2013). Atlas of modern dinoflagellate cyst distribution based on 2405 data points. *Review of Palaeobotany and Palynology*, *191*, 1–198.

How to cite this article: Nag, D., Sangode, S. J., Singh, S. P., Uddandam, P. R., Choudhuri, A., Phartiyal, B., & Prasad, V. (2024). Magnetostratigraphy and rock magnetic studies on the Cretaceous-Paleogene transition strata along the Um Sohryngkew River, Therriaghat, Meghalaya, India. *Geological Journal*, 1–20. https://doi.org/10.1002/gj.5046